AN EXPERIMENTAL-THEORETICAL STUDY OF FREE VIBRATIONS OF PLATES ON ELASTIC POINT SUPPORTS

by

Thomas R. Leuner

AMS Report No. 1052

July 1972

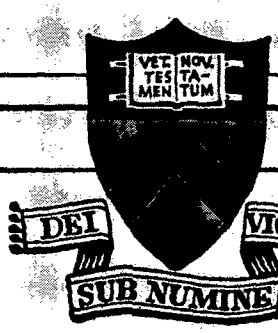

PRINCETON UNIVERSITY

DEPARTMENT OF
AEROSPACE AND MECHANICAL SCIENCES

AN EXPERIMENTAL-THEORETICAL STUDY OF FREE VIBRATIONS OF PLATES ON ELASTIC POINT SUPPORTS

by

Thomas R. Leuner

AMS Report No. 1052

July 1972

ACKNOWLEDGEMENT

I would like to acknowledge the assistance given me by my faculty advisor, Professor Earl H. Dowell. Prof. Dowell not only encouraged and directed me in this research, but since serving as my freshman advisor, has guided me into the field of structural dynamics. I would also like to thank Prof. Robert Mark, who is responsible for my interest in holography. Prof. Mark served as advisor in my holographic studies, which were conducted in the Photomechanics Laboratory of the Civil and Geological Engineering Department.

The experimental program was ably assisted by Mr. Bill James and Mr. Joe Thompson. The manuscript was typed by Miss Bernie Muccilli, for which my wife is extremely grateful.

This research was supported by NASA Grant NGR 31-001-146. A Princeton University Fellowship supported me while I completed this thesis.

This dissertation is dedicated to my wife, Ellen, who contributed mental support and some slave labor towards its completion, but steadfastly refused to let me proofread the manuscript on our honeymoon.

This dissertation carries number 1052-T in the records of the Department of Aerospace and Mechanical Sciences.

ABSTRACT

A theoretical and experimental study is made to investigate the effect on plate vibrations of varying the stiffness of corner elastic point supports. A theoretical model is developed using a Rayleigh-Ritz analysis which approximates the plate mode shapes as products of free-free beam modes. The elastic point supports are modelled both as massless translational springs, and springs with tip masses. The tip masses are included to better represent the experimental supports. An experiment is constructed using the bending stiffness of horizontal beams to support a square plate at its four corners. The stiffness of these supports can be varied over such a range that the plate fundamental frequency is lowered to 40% of the rigid support frequency.

The variation with support stiffness of the frequencies of the first eight plate modes is measured, and compared with the theoretical results. The plate mode shapes for rigid supports are analyzed using holographic interferometry. There is excellent agreement between the theoretical and experimental results, except for high plate modes where the theoretical model is demonstrated to be inadequate.

TABLE OF CONTENTS

NOMENCLATURE

k_{xc}	-	rotational spring stiffness (lbf-in)
k	-	support stiffness (lbf/in)
K_s	=	$k a^2/D$
D	-	plate stiffness
a	-	plate length
K	=	$\omega a^2\sqrt{m/D}$
ω	-	frequency (cps)
m	-	plate mass per unit area (slugs/in^2)
K_{sr}	=	k_{xc}/D
A	-	plate area
E	-	modulus of elasticity
I	-	moment of inertia
L	-	support beam length
μ	-	wire mass per length
w	-	plate deflection
h	-	plate thickness
K_{mn}	-	generalized spring constants
M_{mn}	-	generalized masses
T	-	kinetic energy
U	-	potential energy
X_m, Y_m	-	free-free beam modes
x, y	-	cartesian coordinates

LIST OF FIGURES

CHAPTER I

INTRODUCTION

1.1 Introduction

The purpose of this investigation is to analyze vibrational behavior of plates with discrete elastic supports. Specifically, an experimental model is designed to simulate a square plate with corner elastic supports. Measurements are made to determine the changes in frequency of the natural plate modes as the stiffness of the corner supports is varied. A theoretical model is developed to predict the plate vibration characteristics and the theoretical and experimental results are compared. The mode shapes of the plate vibration are investigated experimentally using holographic interferometry.

The present topic has received little analytical or experimental interest. The vibrations of plates with spring supports is not, however, a topic of purely academic interest. A present candidate NASA Space Shuttle design provides for a thermal protective layer composed of corrugated panels on point supports. The number, location, and nature of these point supports is dependent on the final shuttle design chosen, but at the present time, these supports are not believed to be completely rigid supports. The thermal panels will be supported on structures that can be modelled as springs with finite stiffness.

Due to the difficulty involved in treating corrugated plates theoretically, a flat isotropic plate was chosen for this investigation. The plate was taken to be square to take advantage of symmetry properties, but both the experimental and theoretical programs can easily be expanded to cover rectangular plates. Corner supports were used to facilitate the experimental design, and

to allow comparison with previous work by Reed[1] involving rigid, point corner supports.

Aside from the possible future applications of this research to the vibration of shuttle, and future spacecraft panels, two other factors motivated this study. There is a definite lack of previous work concerning spring supported plates. Another factor affecting the initiation of this research is the previous work done at Princeton by Dowell[2,3,4]. This study is intended to further develop the theory proposed by Dowell in reference 2, and to produce experimental data to compare to this theory.

1.2 Previous Work

The only work known to the author relating the change in plate frequency to the variation in stiffness of point, corner supports is that of Dowell[2]. Dowell calculates the frequency variation of the fundamental plate mode with stiffness using a Rayleigh-Ritz analysis with normal modes of the unconstrained plate. The support conditions are introduced into the analysis by means of Lagrange multipliers.

The theoretical analysis presented in this study is developed from other work by Dowell[4]. This work presents a Rayleigh-Ritz analysis for which support conditions involving point masses and stiffnesses can easily be included. This analysis is then applied to the flutter of a "typical" space shuttle panel.

A number of authors have investigated the problem of a plate with rigid corner supports. Reed[1] presents analytical solutions to plate vibrations using both a Rayleigh-Ritz analysis, and a series solution to the plate equation. The experimental frequencies recorded agree remarkably well with the

theoretical analysis for rigid supports, and Reed's experimental apparatus was used as a basis in designing the experimental setup described in this report.

Tso[5] also presents experimental data for a point supported plate, and this data is compared with energy and finite difference analyses by Johns and Nagaraj[6]. The correlation between theory and experiment is not good, probably due to a lack of convergence in the numerical procedures employed in the theoretical work. Dowell[3] compares the experimental measurements of the plate fundamental frequency from both sources with a revised theory modelling support conditions by Lagrange multipliers. There is substantially better agreement between theory and experiment for this analysis of rigid point supports.

Two general references, Fu-feng[7] and Leissa[8] present information on plates with rigid point corner supports. Fu-feng performs a brief theoretical analysis of the problem using an energy analysis, while Leissa discusses and summarizes the work of previous investigators, including Reed.

Most previous work is only concerned with the fundamental plate mode, and only Reed is concerned with higher plate modes. For the most part, Rayleigh-Ritz analyses are used in these papers. Hopefully, this research will fill some of the gaps left by previous investigators.

1.3 Research Outline

This investigation can be divided into two parts, experimental and theoretical. Each of these parts can be further subdivided. The theoretical analysis of the experimental apparatus poses two models for the support system. One model assumes the supports to be discrete massless elastic springs, while the

other model attempts to compensate for the vibration of real beam-like supports with finite mass. This analysis is presented in Chapter II.

The experimental program described in Chapter III investigates the plate mode shapes and frequencies separately. Holographic interferometry is utilized to investigate the plate mode shapes while the plate frequencies are analyzed conventionally. The experimental results are compared with theory in Chapter IV.

CHAPTER II

THEORETICAL STUDY

2.1 Formulation of Problem

2.1.1 Rayleigh-Ritz Solution

Before the experimental program was initiated, a theoretical analysis was performed to predict the frequency variation of the natural modes of a square plate with the magnitude of the support stiffness of the discrete elastic plate supports. The modal frequencies of the plate were calculated by a computer program utilizing a Rayleigh-Ritz analysis in which the plate modes are represented by the products of free-free beam modes. The relevant equations are presented in Appendix B.

The analysis was programmed so that both rotational and translational springs, and point masses could be added to the plate model at desired positions. To prevent mathematical coupling of uncoupled modes, the vibration of the plate model was divided into four classes of normal modes. The four types of plate vibration are: Class I, modes which are symmetric about both the x and y axes of the plate; Class II, modes which are symmetric about the x axis and antisymmetric about the y axis; Class III, modes which are antisymmetric about the x axis and symmetric about the y axis; and Class IV, modes which are antisymmetric about both the x and y axes. For a square plate, the natural modes and frequencies of Classes II and III are identical.

The plate modes are approximated by combinations of free-free beam modes. Therefore, for Class II solutions, symmetric beam modes are used in the x direction, and antisymmetric beam modes in the y direction, to calculate the mass and stiffness matrices for the unsupported plate.

2.1.2 Support-Plate Interaction

The actual plate support system can be modelled in two different ways. Firstly, it can be assumed that the fundamental frequency of the cantilevered support beam is much greater than the frequencies of the plate modes under consideration. If this condition holds, beam inertia or mass distribution will not affect the natural vibration of the plate and the support beams can be assumed to act as massless translational springs.

It was found, however, that for very low stiffness, corresponding to long beam supports, the frequency of the support beam's first flexural mode was of the same order of magnitude as the frequencies of the higher plate modes studied (see Figure 7). Thus as the plate corners vibrated, the support beams would be oscillated near their fundamental mode, and the mass of the vibrating beams would affect the plate vibration characteristics.

There are a number of ways in which the characteristic vibration of the beam supports could be included in this analysis. The simplest method is to model the support beam as a tip mass, M, on a massless beam with stiffness EI. If EI was selected to be the same as for the actual support beam, the beam model would have the same bending stiffness as the actual support, and the tip mass could be chosen to be the appropriate percentage of the actual beam mass so that the computer model has the same fundamental frequency as the beam support. For a tip mass on a massless beam

$$\omega^2 = \frac{3EI}{ML^3}$$

For a continuous beam with mass,

$$\omega^2 = \frac{12.4\,EI}{mL^4}$$

Equating frequencies

$$M = 0.243\ mL$$

As a second analysis of the plate vibration, the support beams were therefore modelled as vibrating point masses with vertical stiffness.

2.1.3 Selection of Parameters

The input parameters used to generate the theoretical results presented in section 2.1, were selected so that comparisons with available experimental data could be made. The parameters which need be supplied to generate the computer output are; the number of beam modes utilized in the computation, the number and location of discrete point supports, and the values of point masses, translational springs, and rotational springs at these locations. Some difficulties were encountered in selecting these input values due to computational errors involving small differences between large numbers. This problem is discussed in Appendix C. As a result of an analysis discussed in this appendix, two free-free beam modes in each direction were used in the theoretical analysis.

This investigation concentrates on the first eight plate modes: the first three doubly-symmetric plate modes (referred to hereafter as modes one, four, and six), the first two pairs of symmetric-antisymmetric modes (referred to as modes two and three and modes seven and eight), and the first doubly-antisymmetric mode (referred to as mode five). These modes were chosen because they were the subject of previous related analysis by Reed[1], were easily excited and identified experimentally, and the range of frequencies of these modes was, for the most part, below the frequency of the support system.

Dowell's[2] theoretical analysis of this problem, shows that the fundamental plate frequency should reach an asymptotic value for $K_s > 100$. The plate support system was therefore designed to provide non-dimensional support stiffnesses from 2.5 to 100, and this was the stiffness range used in the theoretical computations.

No rotational springs were employed in the analysis, but point mass inputs were needed to simulate the beam vibration. Rather than use linear beam bending theory to calculate the appropriate magnitudes of the beam tip masses for each value of support stiffness used as input, the following procedure was followed. The support system was calibrated (see Appendix D) so that the support stiffness was known for length, L , of the support beams. The support beams were weighed, so the percentage mass of the entire beam which corresponds to each beam length could be determined. In generating the theoretical results, for each value of the support stiffness used as input, the corresponding value of the point mass was determined from the measured beam mass per unit length, and the calibrated beam stiffness per unit beam length.

2.2 Theoretical Results

2.2.1 Plate Frequencies vs. Support Stiffness

The variations of the first eight plate modes with changing support stiffness are presented in Figures 8 through 13. Theoretical results are presented for the two different support models discussed; massless translational springs, and simple beam supports with one lumped mass at the beam-plate junction. On all figures, the theory neglecting support mass effects is represented as a dotted line from K_s equals 0 to 100. Zero stiffness

corresponds to a free support condition of the plate, whereas $K_s = 100$ represents approximately rigid corner point supports. Simple beam support theory is not presented for stiffness values lower than 2.5, which corresponds to the softest support stiffness measured in the experimental program. This simple analysis becomes invalid for very low stiffnesses, because it neglects the effects of higher order beam modes, and hence represents an inaccurate theoretical model.

Figure 8 shows the variation of the first doubly-symmetric plate mode with support stiffness. The non-dimensional plate frequency approaches an asymptote of between 7 and 8 as the support stiffness becomes large, meaning greater than 100. As K_s approaches zero, massless spring support theory predicts that the fundamental frequency of the plate approaches zero. This was the expected result, as the first doubly-symmetric plate mode becomes the translational rigid body mode of the free plate.

Similarly, Figure 9 illustrates the effect of varying support stiffness on the second and third plate modes. These modes have identical frequencies because they belong to Classes II and III for a square plate. These modes do not approach their pin-supported limiting frequencies as rapidly as the first mode, and it appears that the higher the plate mode, the larger the support stiffness necessary to approximate rigid supports. Neglecting the mass of the support system, these modes should correspond to the rotational rigid body modes of a free plate, and as expected, the modal frequencies approach zero as the stiffness of the support system becomes negligible.

The second doubly-symmetric mode is independent of the support stiffness.

Figure 10 shows that the frequency of the fourth plate mode remains constant throughout the range of support stiffness. The reason for this behavior becomes clear after studying the expected mode shape of this mode. The node lines run diagonally between the four corners of the plate. Since the plate is motionless at its four corners, the stiffness of the vertical springs has no affect on the plate vibrations.

The frequency vs. stiffness curves for the fifth through eighth plate modes, Figures 11 through 13, are all qualitatively similar. For negligibly stiff supports, implying free plate boundary conditions, the plate modes begin at finite, non-zero frequencies, and approach higher asymptotic frequencies as the support stiffness is increased. As was previously mentioned, the higher plate modes approach their asymptote more slowly than the lower plate modes.

2.2.2 Comparison of Beam Support Theory with Massless Spring Support Theory

Except for very low, less than $K_s = 2.5$, stiffness, for which the support beam with tip mass model is invalid, the theoretical analyses for both support models are qualitatively similar for all plate modes. However, since beam support theory adds point masses to the plate corners, the more massive plate vibrates at a lower frequency than the plate with massless spring supports. The largest frequency variation occurs for low stiffness, or long support beams, where the mass of the beams becomes appreciable when compared to the plate mass.

Figure 7 shows the variation with stiffness of both plate and support beam modal frequencies. It is evident that for K_s greater than 2.5,

the frequency of the support beam's second flexural mode is more than double any of the plate frequencies under consideration. Modelling the support beams as only vibrating in the first flexural mode is therefore justified.

For the first three plate modes the support beams vibrate at higher frequencies than the plate for the entire stiffness range. Thus compensating for beam vibrations should have only a small effect on the plate frequencies. For $K_s = 2.5$, the frequency of the second and third beam modes is reduced by only 13% when the beam mass is included in the analysis. Since the fourth mode has zero deflection at its corners, the addition of point masses to these locations has no effect on the plate vibration, and the two analyses give the same result.

Plate modes five through eight have higher natural frequencies than the support beams for low stiffnesses. Figure 7 shows that for certain values of stiffness, the beams and plate have the same natural frequency and are in resonance. Introducing beam vibration into the theoretical analysis therefore lowers the plate frequencies significantly. For $K_s = 2.5$, the frequency of the fifth mode is decreased by 23%, the sixth mode by 25%, and the seventh and eighth modes by 27%.

Another consideration is to examine over what range of stiffness the difference between beam support theory and massless spring support theory is significant. As an indication of this, consider the stiffnesses for which the plate modal frequencies are only lowered by 1% when beam mass is introduced to the analysis: for mode one, $K_s = 10$; modes two and three, $K_s = 25$; mode five, $K_s = 66$; mode six, $K_s = 70$; modes seven and eight, $K_s = 83$.

The difference between modelling the support beams as massless translational springs, or as a simple lumped-mass beams, is that for higher plate modes, the vibration frequency of the plate is lowered more, and over a larger range of stiffness when simple beam theory is used. It is expected that the experimental results should agree better with the simple beam theory, which is a closer approximation to the experiment than the massless spring support theory.

2.2.3 Comparison with Previous Work

There are limited published results of similar work with which to compare this theoretical analysis. For a plate on massless point translational springs, the limiting cases of zero stiffness and infinite stiffness can be compared with free plate and rigid corner support results in Leissa[8] and Reed[1] (columns 1 and 3 respectively in the following table).

Since this analysis is inaccurate for large stiffnesses, modal frequencies for K_s = 100 are compared with Reed's rigid frequencies for a general indication of the accuracy of the computation. This comparison is presented in the following table.

Mode	K free plate	$K_s = 0$	K rigid supports	$K_s = 100$
1	0.00	0.00	7.46	6.98
2,3	0.00	0.00	16.80	14.40
4	20.50	22.37	19.60	22.37
5	13.34	13.52	41.50	33.50
6	23.40	22.37	48.30	40.53
7,8	34.70	35.70	51.60	51.32

This data indicates that the theoretical analysis is valid. The largest discrepancy for the zero stiffness results is less than 3%, while the approximately rigid support data compare favorably with Reed's work within the limits of the rigid approximation. Some further work in refining the theoretical model would be worthwhile however.

CHAPTER III

EXPERIMENTAL PROGRAM

3.1 Determination of Modal Frequency Variation with Stiffness

3.1.1 Experimental Arrangement

The design of the experimental apparatus had to satisfy a number of requirements. The primary design condition was to select the size and material for the experimental plate so that it was small enough to have a high fundamental frequency, yet large enough so the plate was not too stiff to measure mode shapes. The plate was finally designed to satisfy the frequency requirement, and an 8" by 8" by 0.125" aluminum (5052 alloy) plate was used in the experiment. This plate would have a fundamental frequency of 146 cps for rigid point corner supports. Thus when the support stiffness was reduced, the frequency of the fundamental mode could be reduced to less than one-third of its rigid value without encountering nonlinearities in the magnetic exciter and capacitive pickup used.

The support system must approximate a point support to the plate. The supports must therefore restrict the vertical motion of the plate corners to be the same as the vertical motion of the supports without restricting rotation of the plate surface at the corners. After an initial design was investigated and discarded, see Appendix E, the final design of this apparatus was adapted from Reed[1].

The four corners of the plate were beveled top and bottom at 35° angles, so that the total included angle of the plate corners was 70°. The plate was supported by the bending stiffness of four horizontal beams, whose protruding ends were routed out to 90° angles. Detailed drawings of the plate

and beam ends are presented in Figures 4a and 4b.

The support beams were aligned along the diagonal axes of the plate. When the beveled plate corners were inserted in the routed beam edges, and the four beams were fastened firmly into position, the extreme corners of the plate were restricted to vibrate vertically with the beams, but the plate was allowed to rotate about a horizontal axis because of the angular difference between the beam and the plate. This is illustrated in Figure 5, a magnified photograph of the junction between the plate and one support beam.

The support beams were designed to have a depth of 0.25", twice the plate thickness, and a width of 0.50" to allow some leeway in the position of the corner of the plate within the beam. These dimensions were also influenced by the requirement that the support beams have a high fundamental frequency. To obtain a non-dimensional support stiffness of 2.5, linear beam bending theory showed that the support beams should be about six inches long. Two additional inches were added to allow for clamping of the beams. The beams were held clamped in support stanchions at a height of four inches over the surface of the base plate. Four inches were allowed so that the magnetic transducer which was used to excite the plate motion could be fastened under the plate. The support stanchions were blocks of aluminum measuring 4-3/8" by 2" by 1-1/2". A rectangular channel housed the support beam which was fastened through the 0.125" thick cover plate by three set screws, located 0.25", 0.75", and 1.75" from the front edge of the stanchion. The bottom of the stanchions were tapped to accept two bolts which passed through the base plate and could be tightened from underneath the plate to clamp the support stanchions into position.

The base plate which supported the experimental apparatus was a heavy aluminum plate 2' by 2' by 0.5". Four quarter-inch wide grooves were routed along the plate diagonals to allow the support stanchions to be fastened at varying distances from the corners of the experimental plate. The base plate was set on wooden blocks to allow access to the support stanchion bolts. The experimental apparatus is shown in Figures 1, 2 and 3.

3.1.2 Support Stiffness Measurement

The spring constant of the support system was determined in the following manner. The stanchion bolts and set screws were loosened so that both the stanchions and the support beams were free to move. The experimental plate was then removed from its supports. The plate was laid on the base plate so that the centers of the two plates coincided, and the experimental plate corners lay along the base plate diagonals. The position of these corners was permanently marked on the base plate, and the experimental plate removed.

The support stiffness was set by placing the front, inward facing edge of the support stanchions a distance L from the marked position of the plate corners. The stanchion bolts were then tightened. The support beams of two adjacent stanchions were clamped by the stanchion set screws so that the beams protruded for a distance, $L + 0.125"$. Due to the routed groove, the point of the groove which contacted the experimental plate, was exactly over the position of the corresponding plate corner.

Two corners of the plate were then placed against the first pair of support beams, and the remaining two beams were moved into contact with the remaining plate corners. The plate was oriented to position its corners approximately in the middle of each support. The second pair of beams was

fastened by pushing each beam firmly against the plate and tightening the rear set screws. The forward set screws were then tightened to lock the support beams into position.

Although this method introduced some compressive stresses in the plate, Reed[1], who performed a similar experiment for rigid corner supports, assumed that the effect of the compressive force was negligible, since it approximated a point load which would produce a small average stress in the entire plate. Appendix D describes the calibration of the support system which relates the stanchion position L, to the measured stiffness of the support beams.

3.1.3 Determination of Plate Modes

Once the stiffness of the support system was measured, the plate was excited by a magnetic transducer, B&K No. MM 0002, powered by a beat frequency oscillator, B&K Type 1022. Small pieces of steel foil were attached to the plate at six different positions for excitation. The expected mode shapes for a square plate with rigid supports were known, and are presented in Figure 14. From these predicted mode shapes, the positions of maximum plate amplitude for the first eight plate modes were determined. These were chosen to be the positions of excitation illustrated in Figure 14. At each of these six positions a hole was tapped in the base plate so the transducer could be fastened at this position.

A framework was attached to the base plate which held a capacitive pickup on a sliding track so it could be positioned over any part of the plate. The output of this pickup was displayed on an oscilloscope so that the plate amplitude was observable. The pickup was positioned over the

transducer in order to observe the maximum plate amplitude. Figure 3 shows the plate exciter and pickup equipment in operation. The plate modes were determined by observing the plate amplitude for resonances as the frequency was varied, and tuning in these resonances to read the modal frequencies.

3.1.4 Plate Frequency Measurement

Working with the theoretical results produced in Chapter II, for each value of the support stiffness investigated, the plate modes were determined as in section 3.1.3. As will shortly be explained the plate mode shapes could not be readily determined by the normal procedure of observing nodal patterns formed with salt or sand.

Instead, for each position of the exciting force, the expected plate resonances were known. Therefore, for a given support stiffness and transducer position, the frequency of the plate mode which should be excited was determined from the analytically predicted results, and the neighborhood of this frequency was searched for a plate resonance. When the resonant frequency was determined, this was taken to be the frequency of the expected plate mode, although the mode shape was not observed at that time. The transducer and pickup were then moved to the next position and the process repeated. In this manner, the frequencies of the plate modes were measured as the support stiffness was varied from 2.5 to 95.

3.2 Determination of Mode Shape Variation with Stiffness

3.2.1 Program Goals

Early investigations of the experimental apparatus showed that the experimental plate was too stiff to vibrate with enough amplitude to form nodal patterns with small salt particles. In order to bounce the salt grains, the

local plate acceleration, $|w(x,y)\omega_n^2|$, must exceed one gravity. Due to the limited power of the transducer and the stiffness of the plate, only for the fourth and sixth plate modes were the amplitude and frequency both large enough to obtain nodal patterns.

To remedy this lack of information on the plate vibration, holographic interferometry was used to determine the plate mode shapes. Basically, holography measures the path length differences between two interfering light beams, and can therefore detect displacements on the order of a wavelength of visible light, which is of the order of one ten-thousandth of an inch.

To measure dynamic displacements, a type of holography known as time-average holographic interferometry is employed. This method can be thought of as measuring the displacement between the maximum excursions of the plate as a double exposure photograph. For more detailed information on holography, see Appendix F, or references 9, 10 and 11.

3.2.2 Holographic Bench Arrangement

This section assumes some prior knowledge of holography in discussing the optics of this experiment. Due to the relatively large size of the experimental plate, and the relatively low power of the eight milliwatt continuous wave laser used, difficulties were anticipated in obtaining good holograms of the entire surface. Therefore this experiment was designed to observe only one-quarter of the plate's surface, and the symmetrical properties of the square plate are utilized in interpreting the entire plate motion.

The base plate of the experiment was modified slightly so that it could be clamped to the holographic bench in a vertical position. Figure 6 shows the position of the vibrating plate and the optical equipment on the bench (scale 1:12). Essentially four factors influenced the experimental design.

The large size of the base plate compared to the bench width hindered the setup, and in order to clamp the plate securely, it had to be placed in the middle of the bench and the laser beams deflected to makeshift bench extensions. The hologram had to be located so there was open area behind it in the laboratory in which the camera could be set up to photograph the holographic images. With the hologram and plate positions set, the spatial filters, which first focus, then diffuse the laser beams had to be set far enough away from the hologram and the plate so they provided even illumination. The prisms and the beam splitter were then positioned to bring the object and reference beams to their respective filters so the total path lengths of these two beams are almost equal. The optical path lengths should be equalized in order that the two beams remain coherent with respect to each other.

In setting up the experiment the surface of the experimental plate was first lightly sandblasted to provide a diffuse optical surface. Black draftsman's tape was used to mark the plate axes around the quadrant to be hologrammed (see Figure 15). The plate supports were adjusted to provide maximum stiffness, $K_s \approx 400$, in the hope of obtaining rigid support mode shapes. The plate was vibrated using the same equipment described in section 3.1, but the capacitive pickup and framework were removed so as not to interfere with the optics.

3.2.3 Experimental Procedure

The experimental results of section 3.1 were used to approximately locate the various plate modes to be hologrammed. Since the capacitive pickup was removed from the system the resonant frequencies were tuned in by ear with the transducer operating at maximum power. The voltage was then adjusted

so the plate vibration could barely be detected with the finger tips. For modes five, six and seven, no vibration could be felt and the transducer output was adjusted to provide between six and ten fringe orders.

Initially, filters were used so that the light intensity due to both the object and reference beams was equal over the entire surface of the photographic plate. Later it was found that brighter pictures were obtained when the filters were removed and the reference beam was approximately 30% more intense than the object beam. Once the laser was adjusted a shutter positioned in front of the laser was closed to cut off the beam.

The experiment was performed in a light and vibration baffled lab. After all lights were blacked out, a photographic plate, Kodak Type 649-F, was installed in the hologram holder, and the laser shutter was opened for the previously determined exposure time, with the plate vibrating the entire time. With the shutter closed, the exposed plate was carried into the darkroom, developed, and hung up to dry.

It was found that even a slightly damp plate obscured the holographic image, and the plate should be completely dry when viewed. Since the hologram reproduces the object beam exactly, the virtual image of the object is located at the object's original position. To photograph the image, focus a camera with high speed film on the object, then turn off all lights and illuminate the hologram only with the reference beam. It should be noted that even holograms which appear dark to the naked eye can register holographic patterns if the camera shutter is left open long enough.

During the course of experimentation, it was found that small changes in the experimental setup could have significant effects on plate exposure

times, object and reference beam intensities, and the darkness of the hologram which effected photographic times. Although it is extremely difficult to recreate holographic results with different equipment, there follows a brief description of the experimental procedure used.

A typical hologram was produced in the following manner using the equipment listed in Appendix A. The reference beam from the eight milliwatt laser was adjusted to be approximately 30% more intense than the reflected object beam (readings of 12 and 9 respectively on a Goffen Luna Pro light meter). The photographic plates were exposed for 50 to 55 seconds, developed for 5 minutes in Kodak D-19 Developer, fixed for 5 minutes using standard Kodak Fixing Agents, and washed in a solution of ethyl alcohol and water (1:1). Pictures of the holographic image were taken using Polaroid Type 57 Film (3200 ASA). The exposure time varied from 2 to 5 minutes depending on the darkness of the developed photographic plate.

As was previously stated, this discussion describes the experimental procedure used assuming a prior knowledge of holography. Further discussion here is not relevant to this investigation, and Appendix F or the references listed may be consulted for a more detailed presentation of the background, theory, and applications of holographic interferometry.

CHAPTER IV

EXPERIMENTAL RESULTS

4.1 Frequency Variation with Stiffness

4.1.1 Introduction

The only previously published results relating plate frequency to support stiffness for corner discrete elastic supports were presented by Dowell[2]. Dowell only presents results for the fundamental plate mode, however, so the only available theory with which to compare the experimental results is that presented in Chapter II. The agreement between the measured plate frequencies and the analytically calculated frequencies is close enough to substantiate both theory and experiment despite the absence of an additional source for comparison.

Figures 8 through 13 compare the measured values of plate frequency with support stiffness against both theoretical results for massless spring supports and simple beam supports. As expected, the experimental results are in closer agreement with simple beam theory, which is a more realistic model of the plate support system.

Within limits, the results presented in this section are repeatable. The major limitation of the experimental program proved to be determining the support stiffness. For the stiffness range $23.5 \leq K_s \leq 59$, the seven data points corresponded to changes in support position of one-eighth of an inch. For changes this small, errors of up to 25% could go unnoticed. The amount of error obviously depends on the precision of the experimenter, but the nature of the experimental apparatus, coupled with the small support changes necessary, must allow for some experimental error in setting the support stiffness.

Two courses of action are open to the experimenter. For each value of support stiffness investigated, the support system could be readjusted until frequencies consistent with theory and other measured frequencies are obtained. This method would furnish experimental results exhibiting a constant trend, although the method of determining support stiffness may vary.

The experimental method used in this investigation was to set the supports for the largest stiffness recorded using the procedure described in section 3.1.2. The plate frequencies were measured and the support stiffness reduced to the next desired stiffness level following the same procedure. In this manner, a set of plate frequencies are generated for the entire stiffness range using identical methods for each value of support stiffness. Although certain data points may not exactly follow the general experimental trend, the data set presented is as a whole more consistent.

The data presented in this section are the experimental frequencies measured having the fewest deviations from the general trend of the data. For most of the plate modes presented in Figures 8 through 13, plate frequencies for support stiffness $K_s = 59$, appear lower than the other measurements would predict, and frequencies corresponding to $K_s = 23.5$, appear higher than the general trend. This is presumably caused by errors in determining these support stiffnesses, and the support system is actually softer in the first case, and more rigid in the second case, than the stiffness calibration indicated.

4.1.2 Comparison with Theory

The frequency vs. stiffness variation of the first plate mode is illustrated in Figure 8. The largest quantitative difference between experiment

and theory is 5%. For stiffnesses of $K_3 < 20$, the agreement between experiment and theory is excellent, although for larger stiffnesses the theoretical results appear to be conservative. The qualitative agreement is good however, and energy methods like the Rayleigh-Ritz analysis used are expected to overestimate system eigenvalues.

The experimental results presented in Fig. 9 follow the same pattern as the fundamental mode frequencies. As the support stiffness is varied, the frequency of modes two and three increases qualitatively with the theoretical result assuming the support beams to be stiff rods with tip masses. The maximum quantitative difference is 4%, and the experimental and theoretical results are in better agreement for $K_3 < 30$, than for higher stiffnesses where the theoretical results overestimate the experimental.

It should be noted that for $K_3 < 25$, the experimental frequencies are bracketed between theoretical results for massless spring supports, and simple beam with tip mass supports. This indicates that lumping the beam mass into one point mass at the plate corner may be a crude approximation overestimating the correction needed to account for vibration of the support beams.

The experimental results presented in Fig. 10 prove that the frequency of the fourth plate mode is independent of the support stiffness. This was predicted by theory, but there is a large discrepancy in the magnitude of the plate frequency. This, however, seems to be an inaccuracy of the analysis, since Reed[1] predicts $K_4 = 19.6$, and the measured frequency was found to be $K_4 = 19.3$. Again, the theory is conservative.

The fifth plate mode shows the best correlation between experiment and theory. The maximum differential between experimental frequency and the predicted value plotted on Fig. 11 is 2%. For most values of the support

stiffness, the measured plate frequency is higher than that predicted by assuming the support beam to be a flexible rod with tip mass, but less than the theoretical frequency for a plate on massless spring supports. This confirms the assumption that lumping the beam mass is an overestimation of the support vibration correction.

The experimental plate frequencies plotted in Fig. 12 behave in a manner similar to that of Fig. 11, but the discrepancy between theory and experiment is greater for the sixth mode as opposed to the fifth plate mode. The largest quantitative difference is 5%.

Plate modes seven and eight exhibit the worst correlation between theoretical and experimental results as shown in Fig. 13. The experimental plate frequencies plot as a smooth curve over the entire stiffness range, and are in reasonable agreement with theory for $K_s < 20$. For higher stiffnesses, however, theoretical analysis exceeds the experimental results by about 10%.

4.1.3 Discussion

As has previously been mentioned, and will be more fully discussed in Appendix C, there are inaccuracies in the theoretical solution which could easily be the source of the behavior of modes seven and eight. Section 2.2.1 discusses how the higher the plate mode, the slower the mode to approach its rigid support frequency. Referring to the table in section 2.2.3, the values of theoretical stiffness for $K_s = 100$ as percentages of the frequencies predicted in Leissa[8] for rigid supports are: mode one, .936; modes two and three, .857; mode five, .808; mode six, .840; modes seven and eight, .995.

These percentages should decrease as the mode number increases. Therefore, although only the end points of the theoretical curves are being

discussed, it seems that theory for the sixth plate mode slightly overestimates previous theory, and should therefore overestimate the experimental results. Similarly, the theoretical analysis for modes seven and eight predicts frequencies significantly higher than that indicated by Leissa. Thus the experimental frequencies for these modes would hopefully be in better agreement with an improved theoretical calculation.

In general, there appears to be excellent agreement between the experimental results and the theoretical analysis modelling the support beams as springs with point masses at the plate corners. Discrepancies are observed at high stiffnesses due to the conservative nature of the Rayleigh-Ritz analysis, and for high plate modes due to inaccuracies in the theoretical computations.

4.2 Plate Mode Shapes

4.2.1 Introduction

One of the advantages of holographic interferometry over conventional node line analysis, is that relative peak-to-peak vibration amplitudes can be measured over the entire plate surface. Originally, it was intended to quantitatively compare plate mode shapes for rigid and soft plate support systems. This proved to be impossible, however, since holograms showed modes two and three and modes seven and eight to be coupled. Due to the low intensity of the laser beam, a clear hologram of the first mode, which has no bright node lines, could not be obtained over the entire plate quadrant. The only remaining plate mode whose shape would be significantly effected by a stiffness variation was the sixth mode.

Fortunately, the sixth mode node lines could be obtained by bouncing

glass beads on the plate surface in its horizontal position. Thus the plate mode shapes were investigated holographically only for approximately rigid supports (K_s = 400). Figures 18 and 21 show the variation in node line position for modes four and six as the support stiffness is changed from K_s = 400 to K_s = 5. Since the fourth mode is independent of the support stiffness, the node lines are the same for both stiffness values. Figure 21 shows that as the support stiffness is decreased the diameter of the circular node line of the sixth plate mode increases from about 58% of the plate width to 76% of the plate width.

Figures 16, 17, 19, 20, 22 and 23 are photographs of the hologram mode shapes. To interpret these mode shapes, Fig. 15 should be consulted to determine the plate center, support position, and axes system for the plate quadrant photographed. The theoretical frequencies and mode shapes are presented in Fig. 14. The frequencies of the observed mode shapes compare favorably with the theoretical frequencies, and the mode shapes will be discussed in the following section.

4.2.2 Analysis of Mode Shapes

The mode shape of the first plate mode is shown in Fig. 16. Appendix F describes how nodal lines of the plate vibration are distinguished by very bright interference fringes, and as the amplitude of the plate vibration increases, the intensity of the light fringes decreases. There are no node lines in the plate fundamental mode, and the hologram is consequently so dark that the center fringe orders are barely observable. To photograph the hologram, the center of the plate was artificially lightened to provide a better picture.

The observed mode shape agrees with that predicted in Fig. 14. The plate displacement is zero at the support position, and increases towards the center of the plate. Due to the darkness of the hologram, it was impossible to determine whether the maximum displacement amplitude occurred at the exact plate center.

Figure 17 shows the observed mode shape of the second plate mode. This antisymmetric-symmetric mode should exhibit a node line along the entire Y axis. The observed node line originates in the negative X , negative Y quadrant of the plate (refer to Fig. 15 nomenclature), crosses the Y axis near the plate center, and continues into the positive X , positive Y quadrant.

This mode shape is disappointing but explainable. If the position of the exciting force was slightly off the desired location, or if the corner supports were not all identically stiff, a coupled mode could be excited. If this coupled mode was a combination of antisymmetric-symmetric mode two and symmetric-antisymmetric mode three, which both have identical frequencies, the coupled mode shape could be as that observed. An attempt to examine the mode shape of mode three produced no additional information, since that mode also appeared coupled and no nodes were visible in the quadrant hologrammed.

The mode shape of the fourth plate mode, Fig. 19, is exactly as anticipated. The node line begins at the plate corner, and follows the diagonal to the plate center, where node lines from the other corners also end.

The node lines of the fifth plate mode do not precisely match the theoretical mode shape. Figure 20 shows the node lines do not follow the X and Y axes as theory predicts, but form two hyperbolas in the positive X , positive Y and negative X , negative Y plate quadrants. These hyperbolas

intersect, and follow the axes at a distance of about one-eighth the plate width from the center. This deviation from the expected mode shape could be caused by unequal support stiffness allowing slight plate vibration at the center.

The sixth plate mode, Fig. 22, exhibits the clearest node line. The measured node line is a circle, as is predicted by theory, with a diameter equal to 64% of the plate width. The maximum amplitude of this mode is observable at the plate center, where the intensity is low due to the relatively large fringe order at that point.

Following the same analysis used in discussing the mode shape of mode two, Fig. 23 shows the mode shape of mode seven to be coupled with that of the eighth plate mode. One node line should follow the negative Y axis, and the second should begin at the plate corner and curve upwards to intersect the positive X axis. Instead, these lines are skewed in a counterclockwise direction, presumably due to a combination of effects stemming from uneven support stiffnesses or an improperly placed driving force.

4.2.3 Discussion

Although the original program of analytically measuring the exact mode shapes for various stiffnesses could not be completed, holography was shown to be a useful experimental tool. Even though the skewed mode shapes for the coupled modes could provide no useful displacement measurements, this does not mean that the modal frequency measurements were in error.

Theoretical investigation showed that 20% variations in the values of the stiffnesses of the individual corner supports had negligible effect on the modal frequencies as long as the average stiffness of the four supports

remained constant. This mode shape investigation indicates that the plate mode shapes are more dependent on the stiffness of the individual plate supports than the frequencies of the plate modes.

An extensive holographic investigation could determine and isolate the source of the mode couplings, and obtain clearer, measurable holograms. This investigation would involve a great amount of time and expense, however, for the production of a single hologram takes one hour from exposing the plate until the hologram is dry enough to be examined. Real-time holography might be used, in which a hologram of the stationary object is made, and replaced in its exact original position. Interference fringes are then observable as the plate is vibrated due to interference with the processed hologram. Effects of adjusting the corner supports would be instantaneously observable without producing time-average holograms of unseen vibrations. However, clear photographs may still require time-averaged hologram production (see Ref. 10).

CHAPTER V

CONCLUSIONS AND RECOMMENDATIONS

5.1 Conclusions

This study did not completely accomplish its original objective: to experimentally investigate the vibration of a plate on discrete elastic supports. It was found that the support system interacted with the plate for soft supports, and the vibration of the experimental support beams effected the vibration of the plate. Given this experimental limitation, a theoretical analysis was developed which successfully predicted the plate vibration for the first five plate modes. For higher plate modes, the theoretical analysis was shown to be somewhat inaccuate, presumably due to computational difficulties involving small differences between large numbers.

While the experimental apparatus did not successfully provide massless elastic supports to the experimental plate under all conditions, it did approximate point corner supports well. The apparatus produced consistent and reproducible results, with the major limitation being the experimenter's accuracy in setting the support stiffness.

Holographic interferometry proved to be a useful tool in investigating plate vibrations. The applications of holography were not deeply investigated, and more experience with the technique, coupled with more refined equipment could probably produce better mode shape pictures.

5.2 Recommendations

The results of this investigation leave four areas open for further research. Firstly, a theoretical analysis should be developed which accurately

predicts the plate frequencies for high modes and stiffnesses. Secondly, a new experimental apparatus should be designed for which vibrations of the support system do not violate the assumptions of massless elastic supports. Two possible supports recommended are: 1) an optimization of the beam support dimensions to provide minimum stiffness with maximum frequency, and 2) further development of the wire support system investigated in Appendix E. The width and depth of the support beams could be adjusted to provide maximum fundamental frequencies for desired stiffness values, but this would have a small effect, and the same problems would be encountered for slightly softer supports. Since the mass of the support wires were substantially less than the corresponding mass of the support beams, this method of support might have less effect on plate vibrations. The last recommendation for future research is that a more extensive investigation of the plate modes using holographic interferometry be undertaken to determine the source of mode shape irregularities in the apparatus.

REFERENCES

1. Reed, Robert E., Jr., "Comparison of Methods in Calculating Frequencies of Corner-Supported Rectangular Plates", NASA TN D-3030, Sept. 1965.

2. Dowell, E. H., "Free Vibrations of an Arbitrary Structure in Terms of Component Modes", Journal of Applied Mechanics, ASME, No. 72-APM-T, 1972.

3. Dowell, E. H., "Free Vibrations of a Linear Structure with Arbitrary Support Conditions", Journal of Applied Mechanics, Vol. 38, Sept. 1971, pp. 595-600.

4. Dowell, E. H., "Theoretical Panel Vibration and Flutter Studies Relevant to Space Shuttle", AIAA Paper No. 72-350, April 1972.

5. Tso, W. K., "On the Fundamental Frequency of Four Point-Supported Square Elastic Plate", AIAA Journal, Vol. 4, No. 4, April 1966, pp. 733-735.

6. Johns, D. J. and Nagaraj, V. T., "On the Fundamental Frequency of a Square Plate Symmetrically Supported at Four Points", Journal of Sound and Vibration, Vol. 10, Nov. 1969, pp. 404-410.

7. Fu-feng, Chang, "Thin Elastic Plates", Air Force Systems Command, FTD-TT-65-157, April 4, 1966.

8. Leissa, Arthur W., "Vibrations of Plates", NASA SP-160, 1969.

9. Collier, R. J., Burckhardt, C. B. and Lin, L. H., Optical Holography, Academic Press, New York, 1971.

10. Evensen, D. A. and Aprahamian, R., "Applications of Holography to Vibrations, Transient Response, and Wave Propagation", NASA CR-1671, Dec. 1970.

11. Horvath, V. V. and Wallach, J., "Holographic Interferometry Applied to Experimental Mechanics", General Electric Report No. 70-C-352, October 1970.

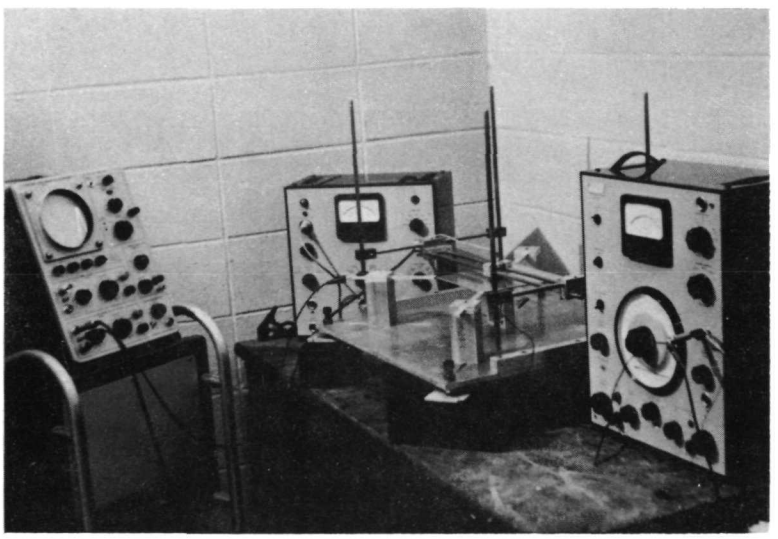

GENERAL VIEW OF EXPERIMENTAL EQUIPMENT

FIGURE 1

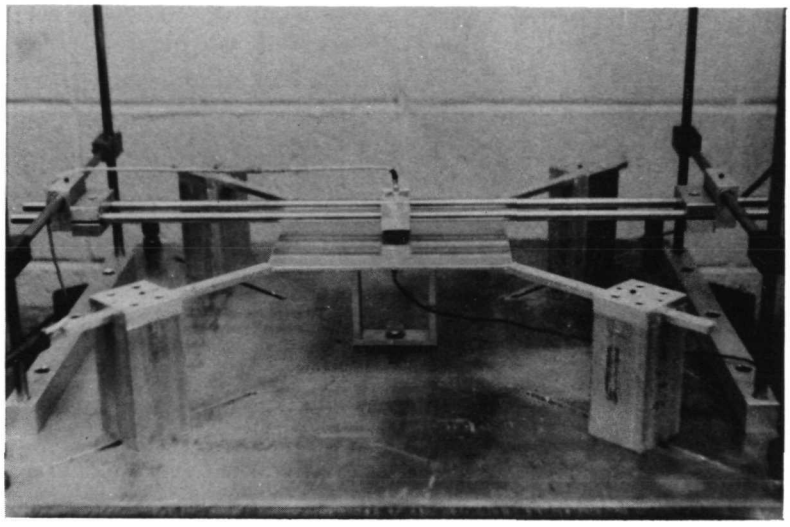

PLATE AND SUPPORT SYSTEM

FIGURE 2

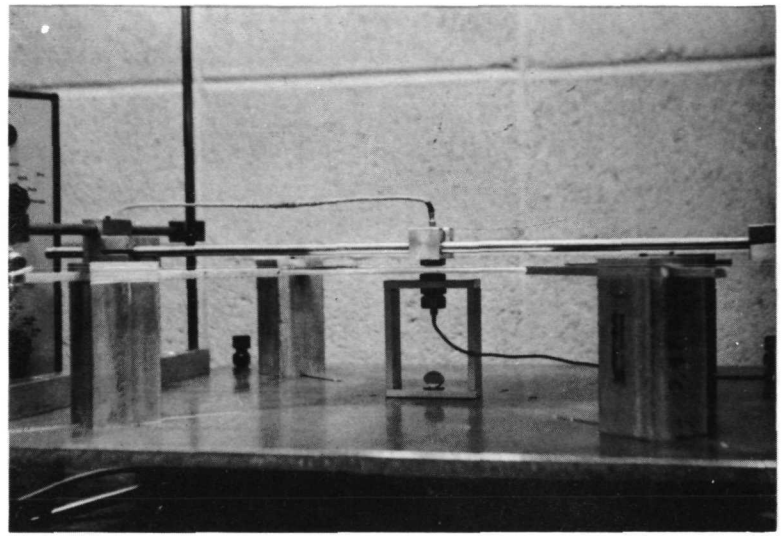

SIDE VIEW OF PLATE EXCITER
AND DISPLACEMENT TRANSDUCER

FIGURE 3

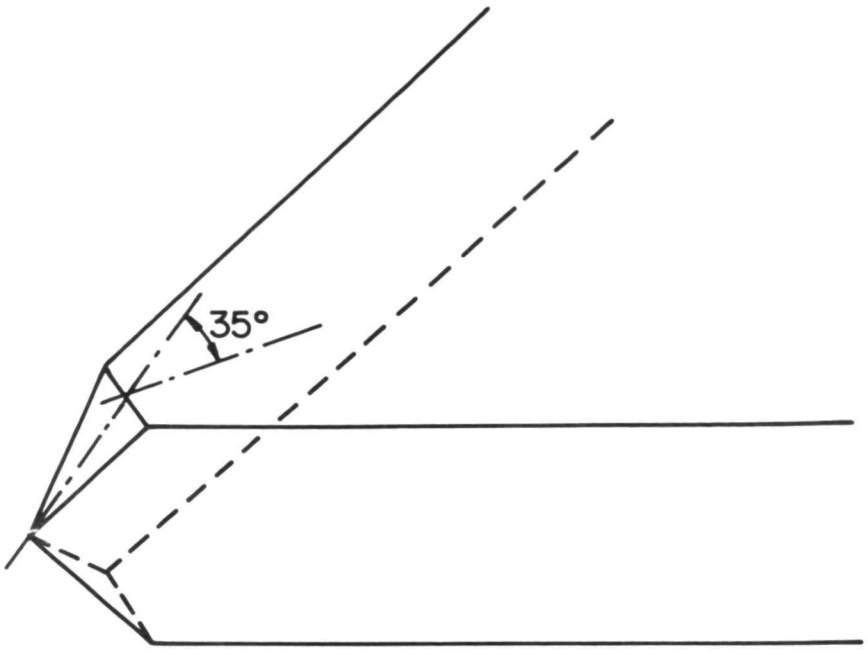

a) DETAIL OF PLATE CORNER

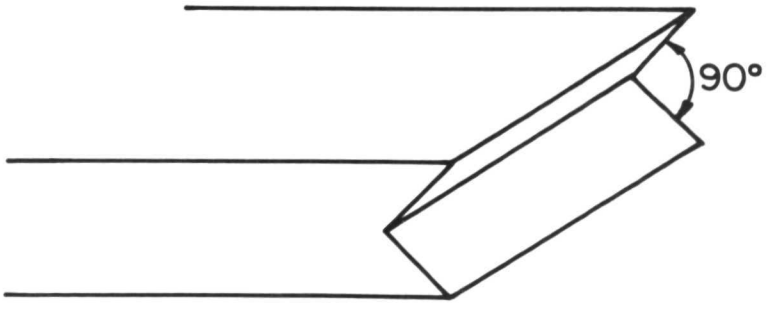

b) DETAIL OF SUPPORT BEAM EDGE

FIGURE 4

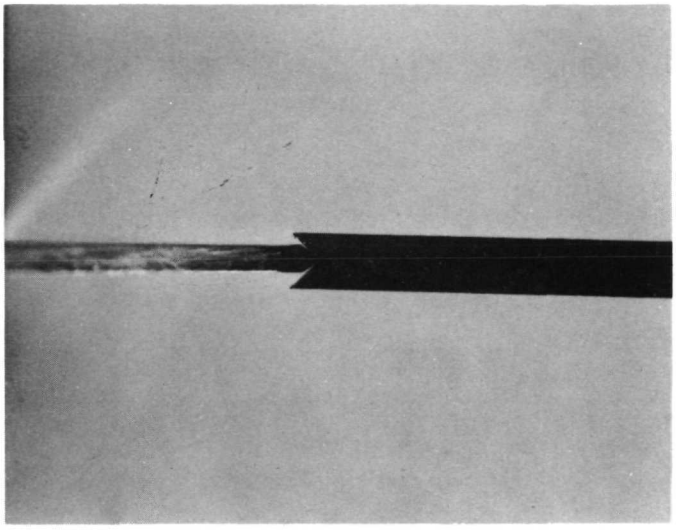

MAGNIFIED VIEW OF PLATE
AND SUPPORT BEAM JUNCTION

FIGURE 5

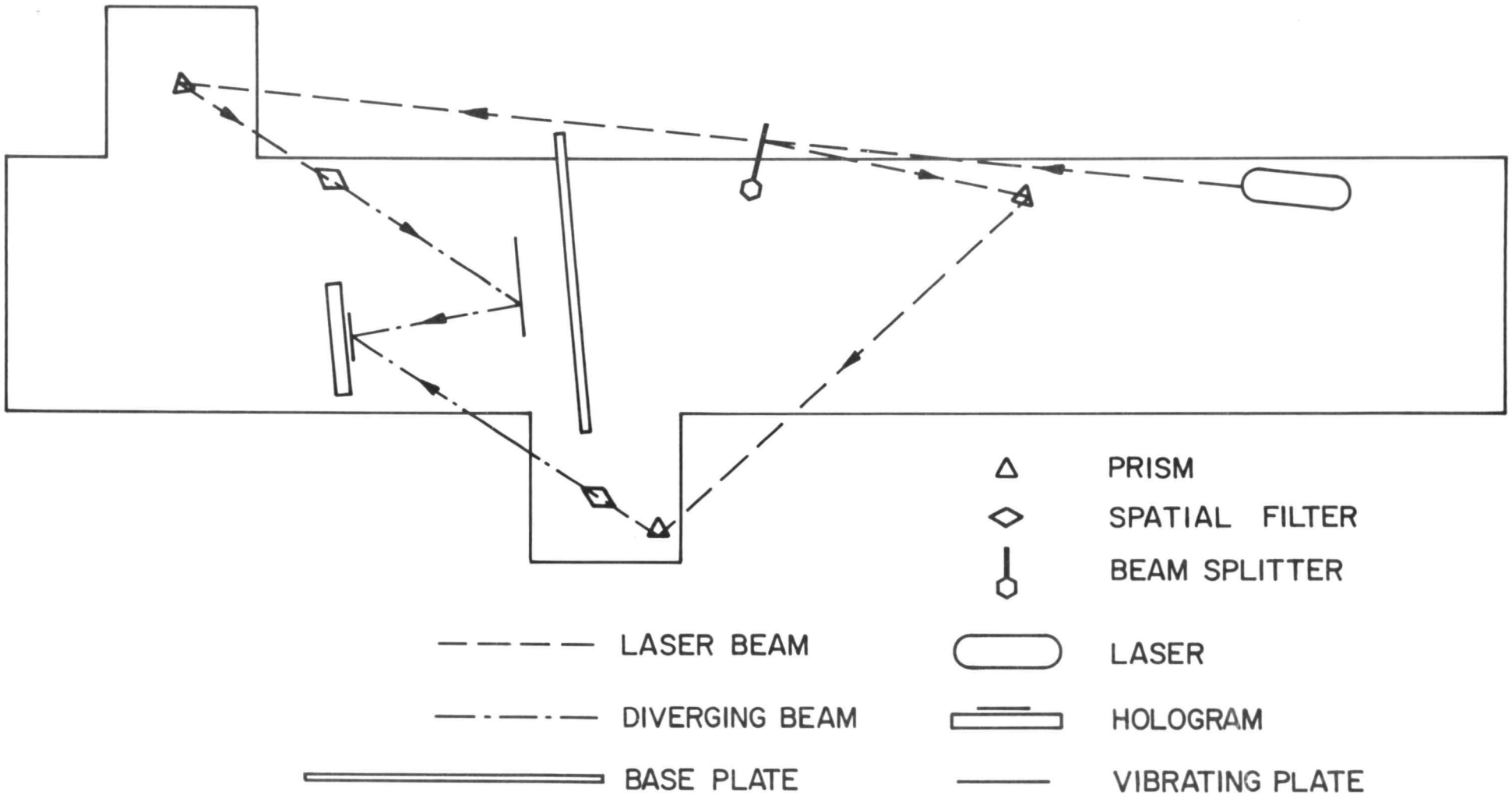

OPTICAL ARRANGEMENT OF HOLOGRAPHIC BENCH

FIGURE 6

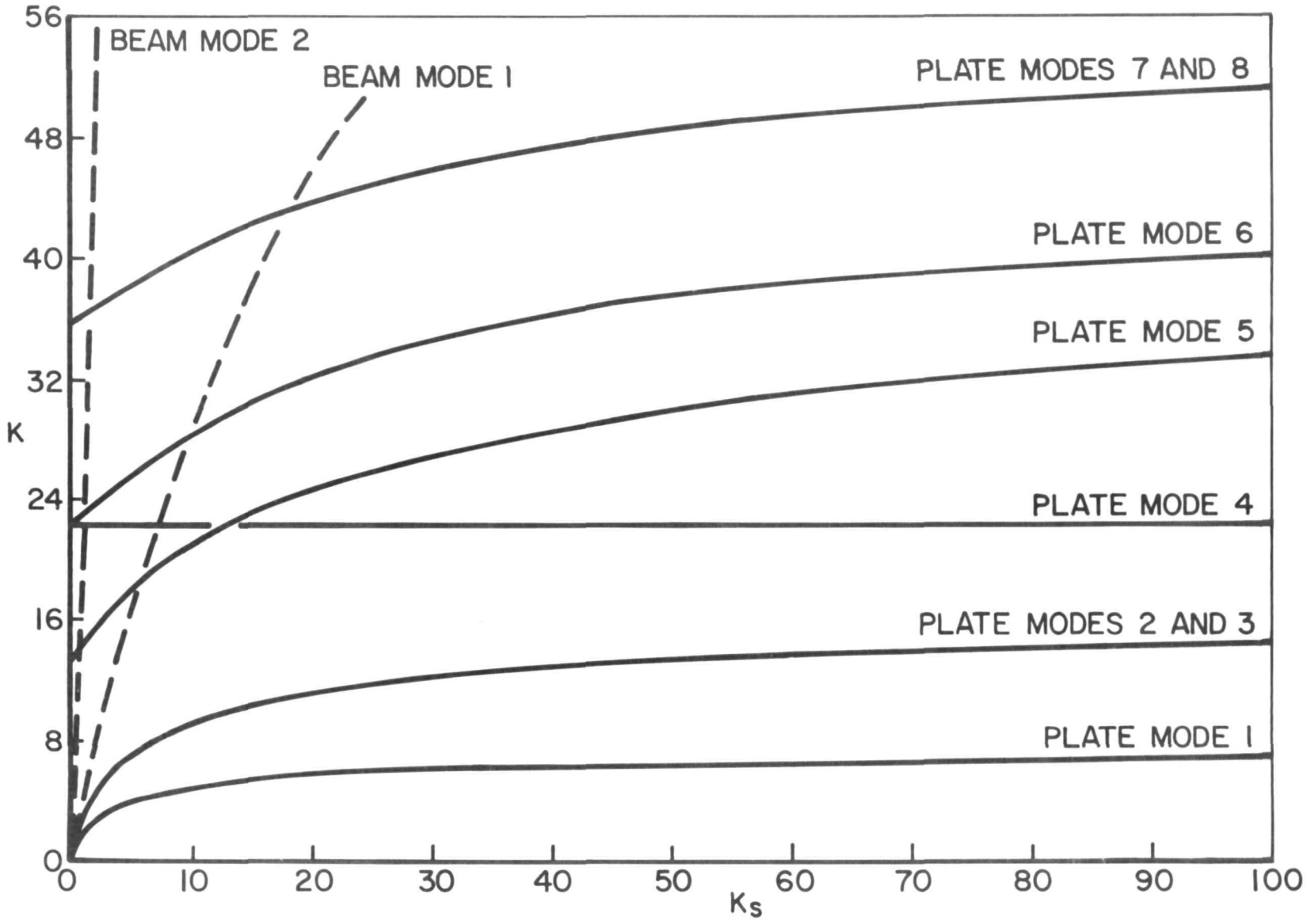

FREQUENCY vs STIFFNESS OF SUPPORT BEAM AND PLATE MODES

FIGURE 7

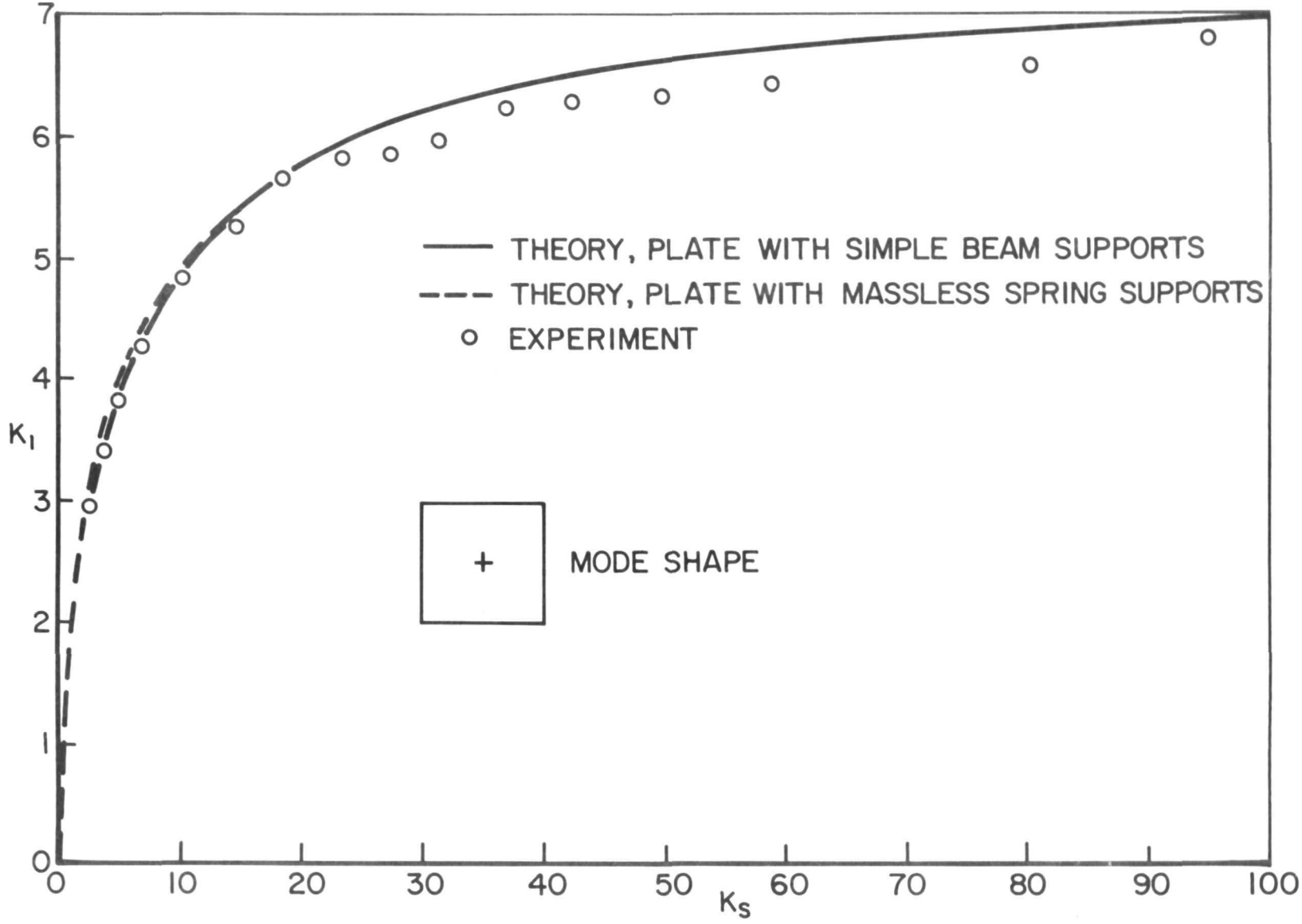

FREQUENCY vs SUPPORT STIFFNESS, FIRST MODE

FIGURE 8

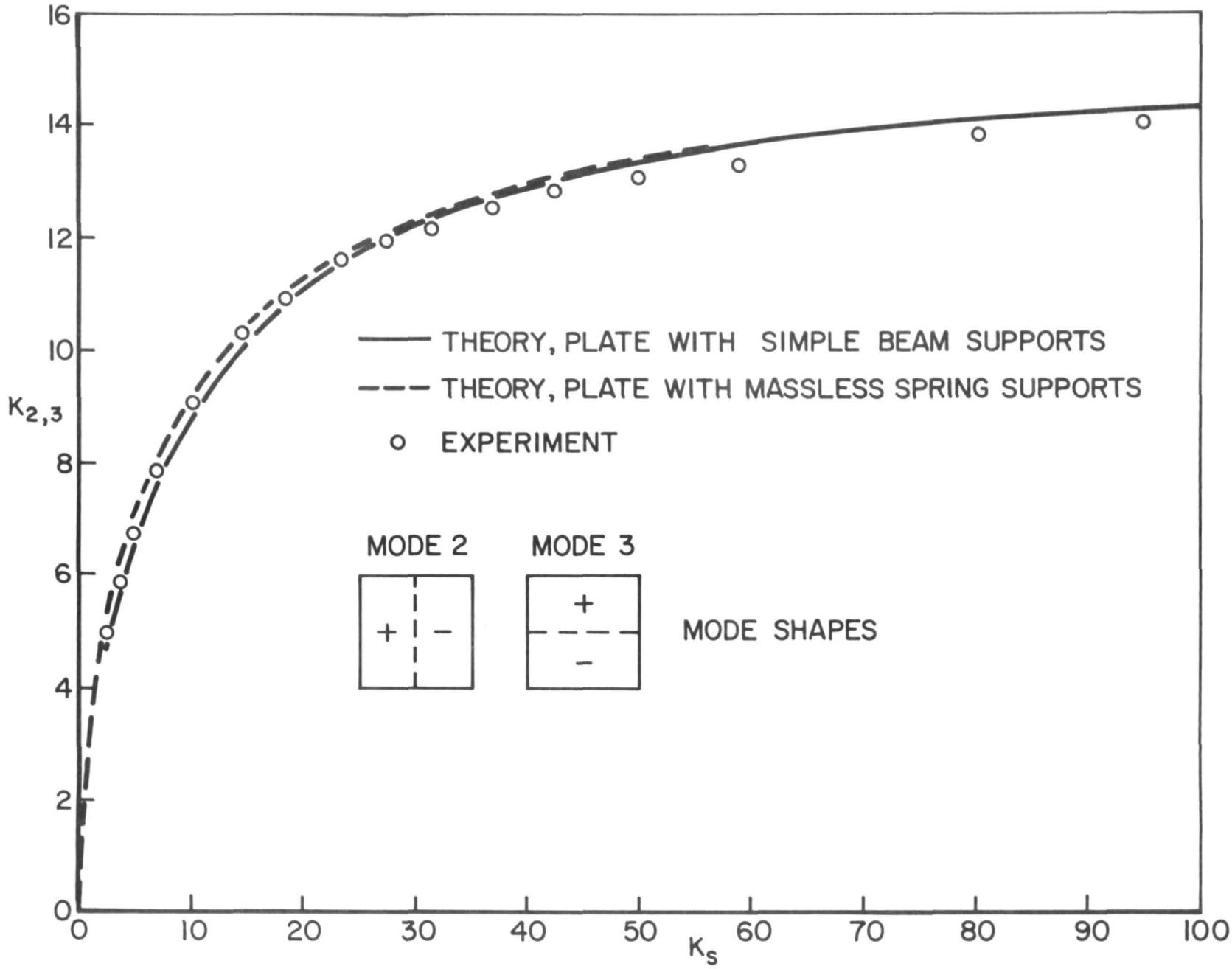

FIGURE 9

FREQUENCY vs SUPPORT STIFFNESS, SECOND AND THIRD MODES

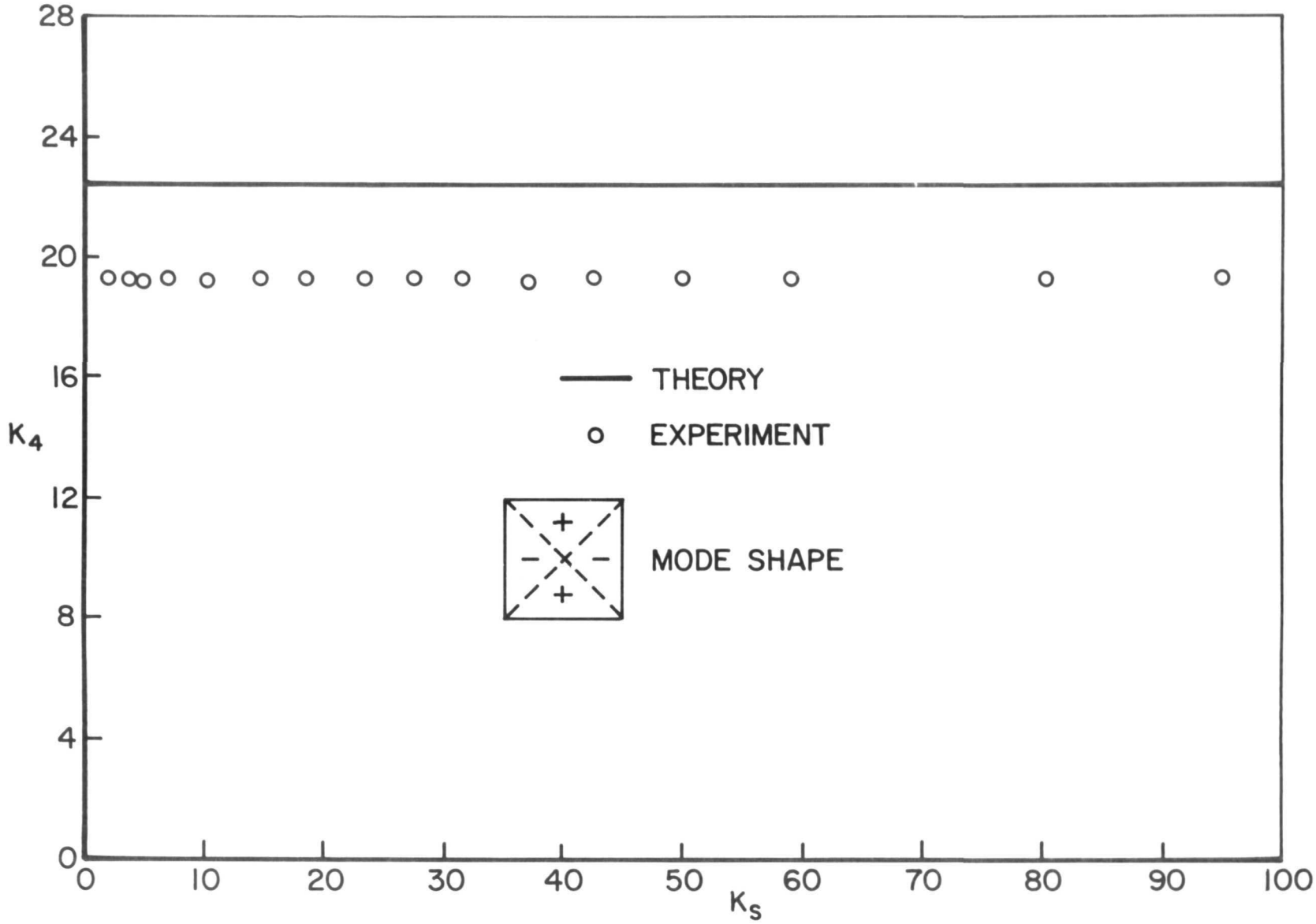

FREQUENCY vs SUPPORT STIFFNESS, FOURTH MODE

FIGURE 10

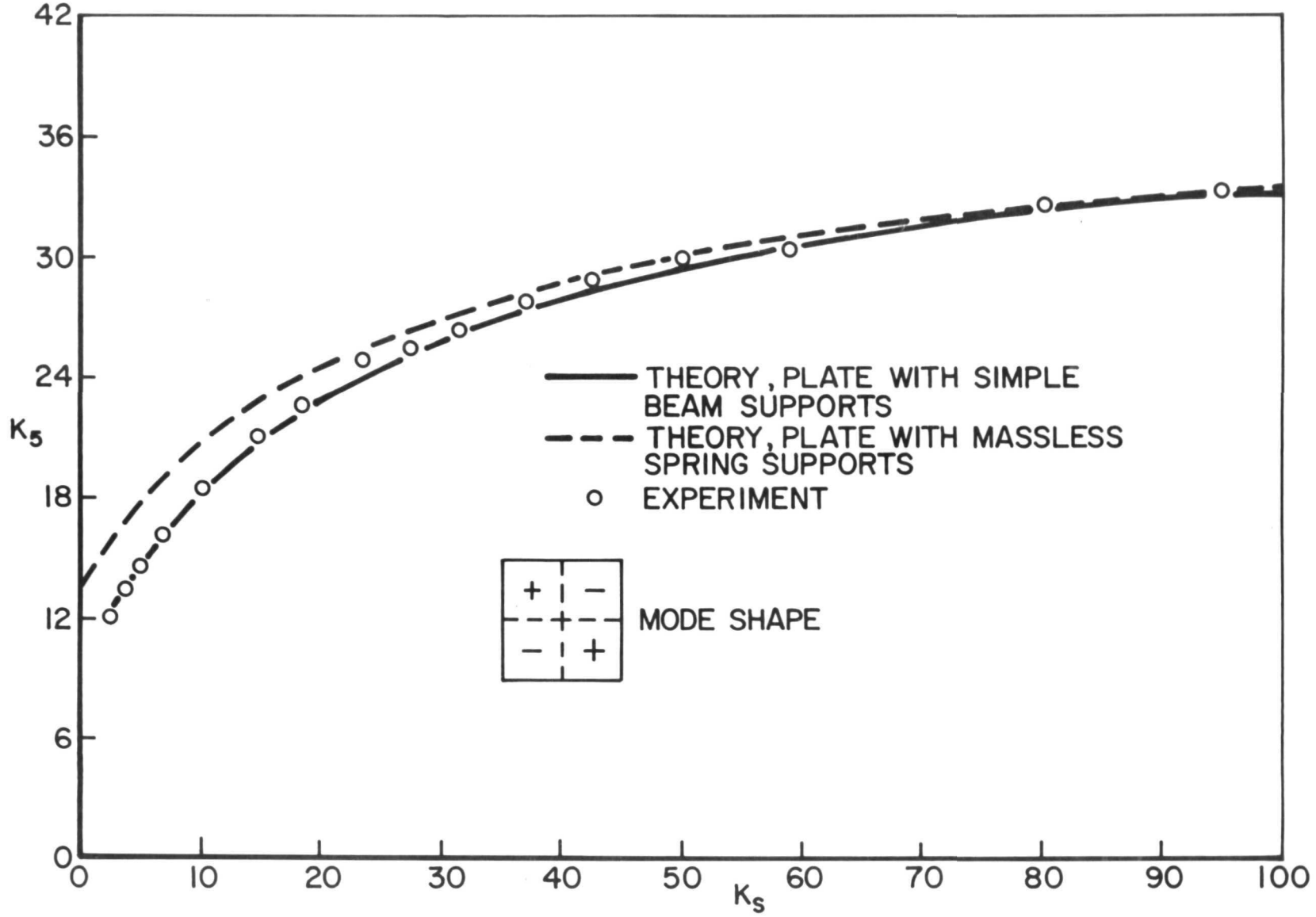

FREQUENCY vs SUPPORT STIFFNESS, FIFTH MODE

FIGURE 11

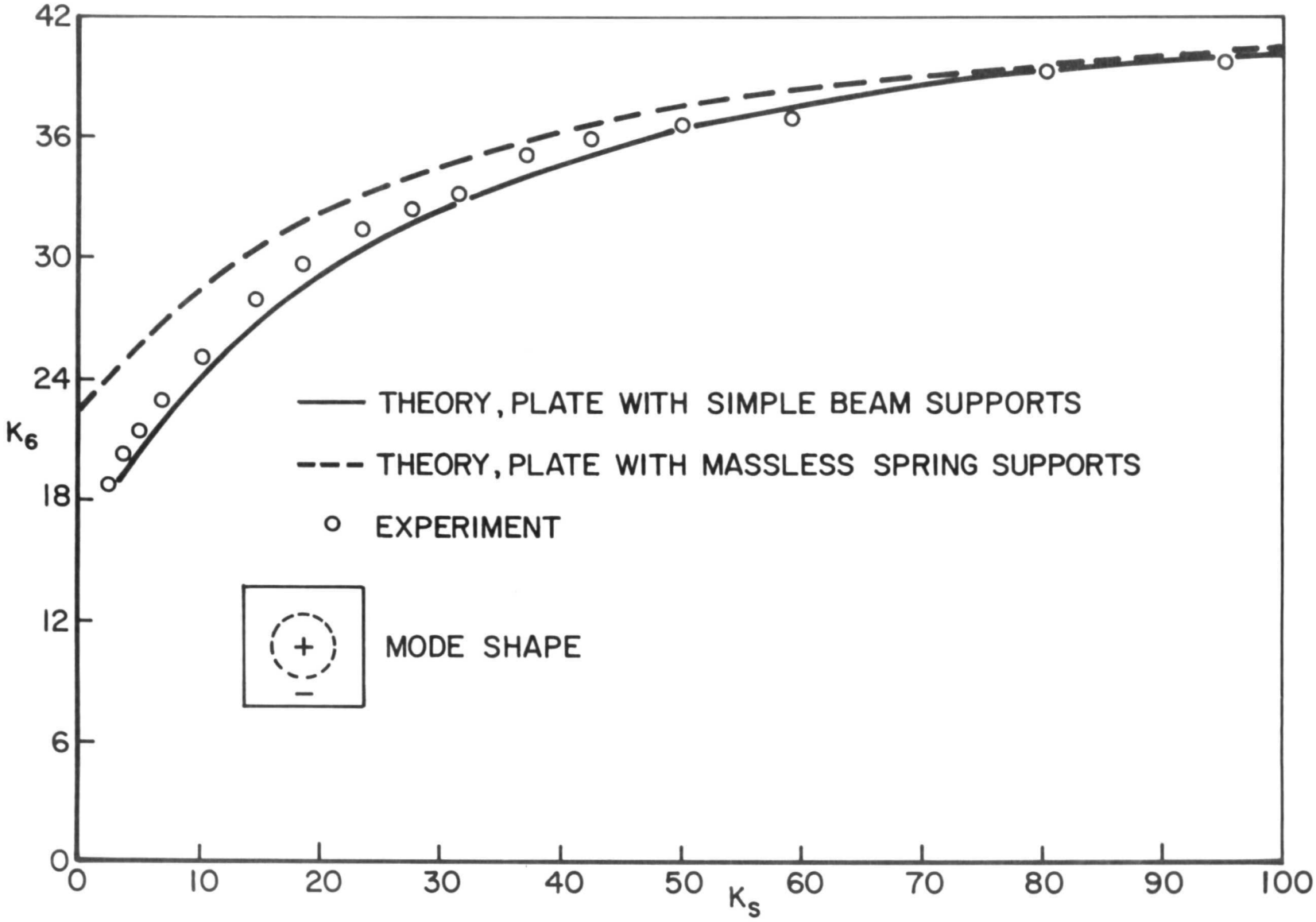

FREQUENCY vs SUPPORT STIFFNESS, SIXTH MODE

FIGURE 12

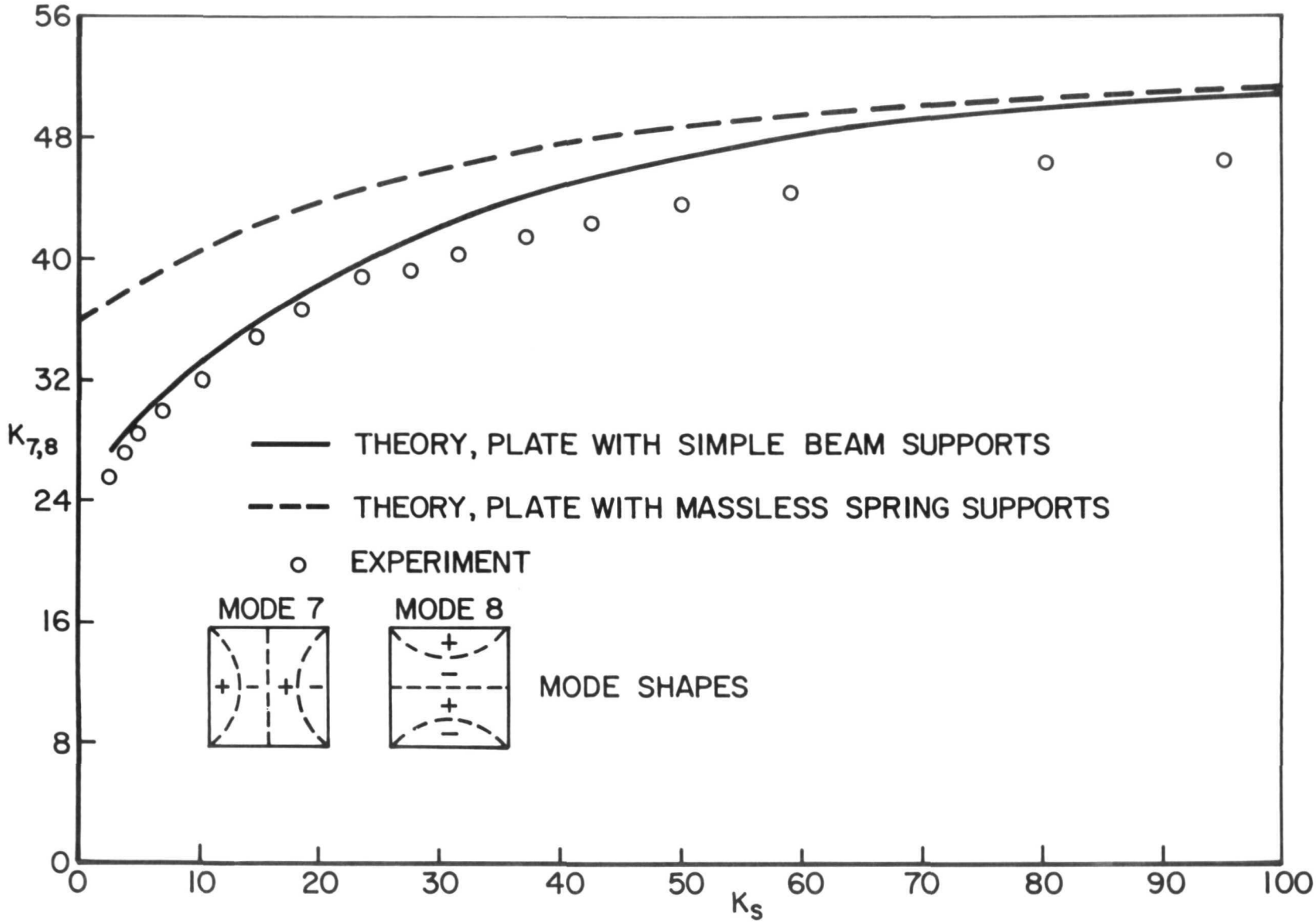

FREQUENCY vs SUPPORT STIFFNESS, SEVENTH AND EIGHTH MODES

FIGURE 13

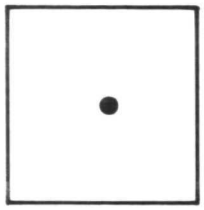

$\omega_1 = 143$ cps

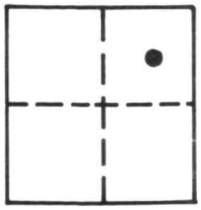

$\omega_5 = 724$ cps

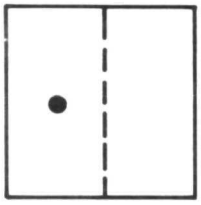

$\omega_2 = 300$ cps

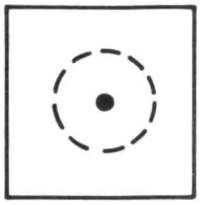

$\omega_6 = 851$ cps

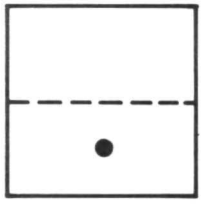

$\omega_3 = 300$ cps

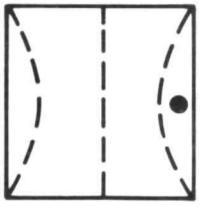

$\omega_7 = 1044$ cps

$\omega_4 = 439$ cps

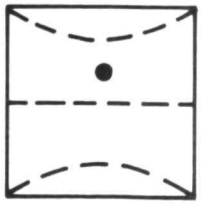

$\omega_8 = 1044$ cps

• LOCATION OF DRIVING FORCE

THEORETICAL MODE SHAPES AND FREQUENCIES FOR APPROXIMATE RIGID SUPPORTS

FIGURE 14

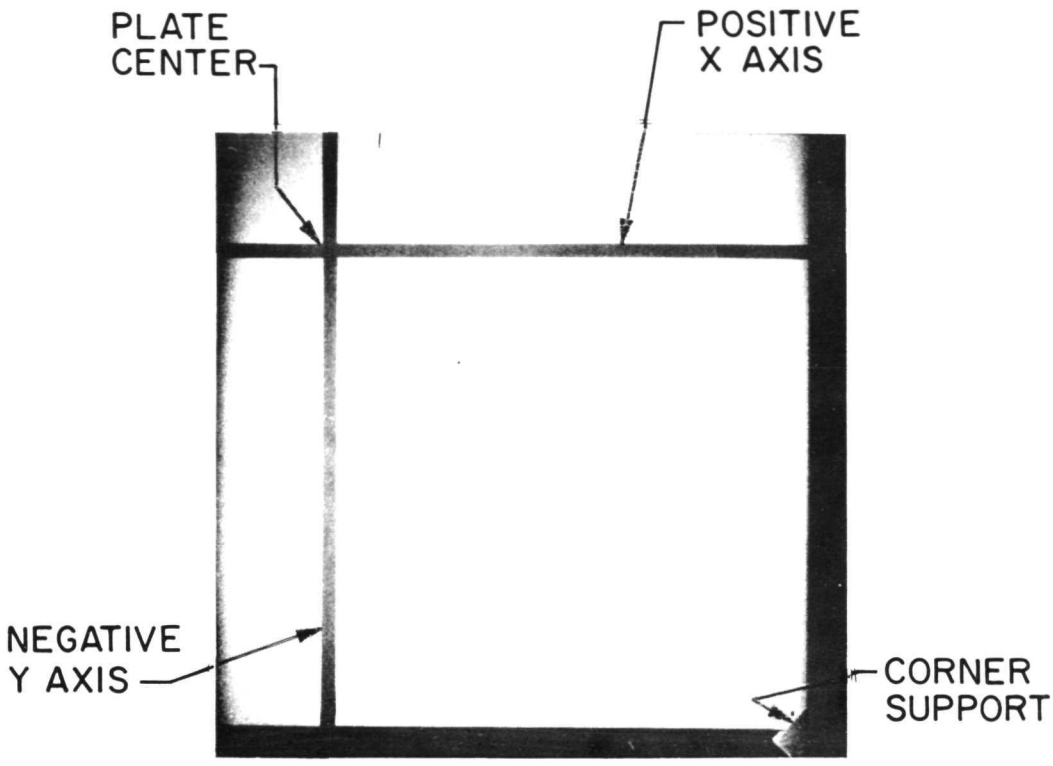

PLATE QUADRANT AND AXIS SYSTEM

FIGURE 15

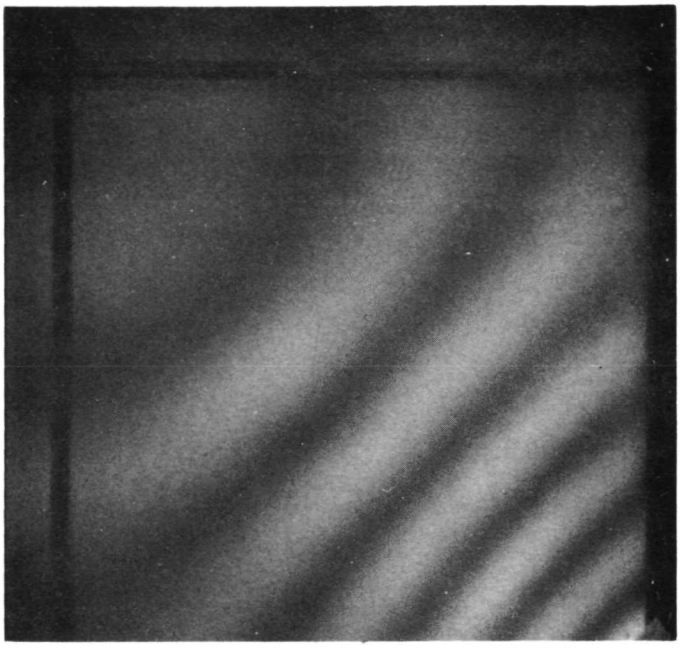

MODE SHAPE OF FIRST MODE
$K_s = 400$, $\omega_1 = 152$ cps

FIGURE 16

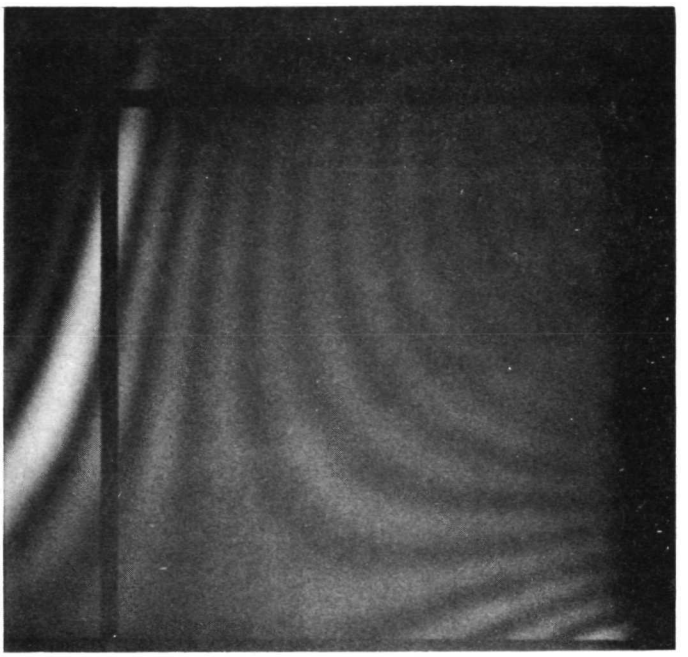

MODE SHAPE OF SECOND MODE
$K_S = 400$, $\omega_2 = 306$ cps

FIGURE 17

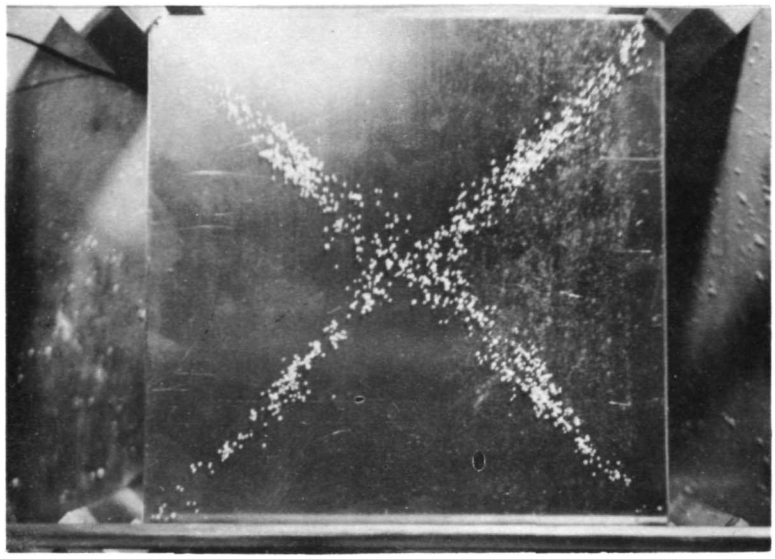

$K_s \approx 400$ $\omega = 378$ cps

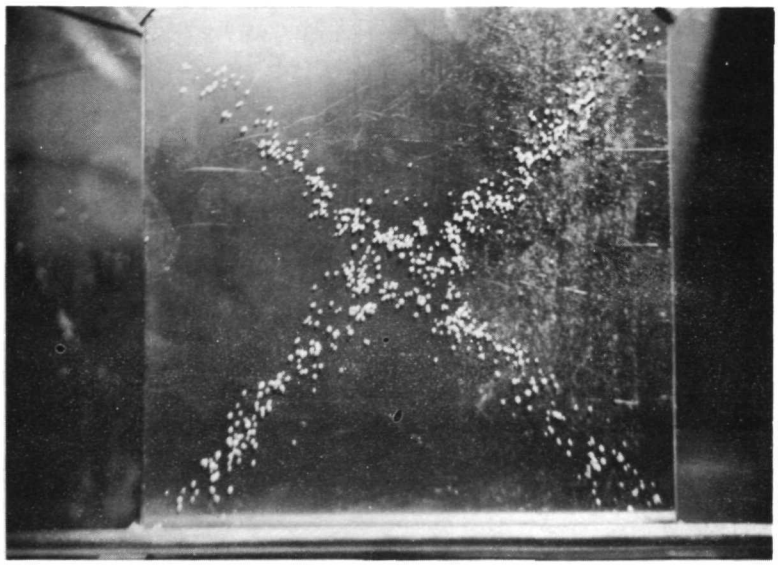

$K_s \approx 5$ $\omega = 378$ cps

EFFECT OF SUPPORT STIFFNESS ON MODE SHAPE, FOURTH MODE

FIGURE 18

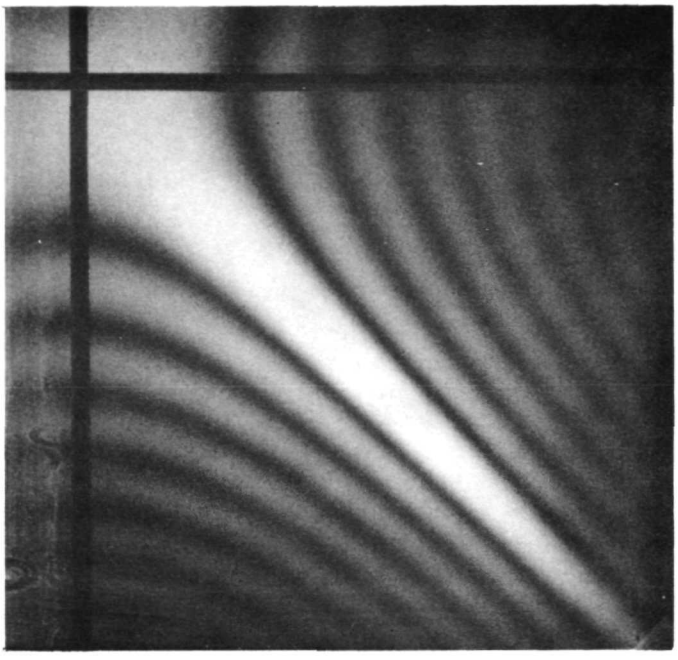

MODE SHAPE OF FOURTH MODE
$K_S = 400$, $\omega_4 = 392$ cps

FIGURE 19

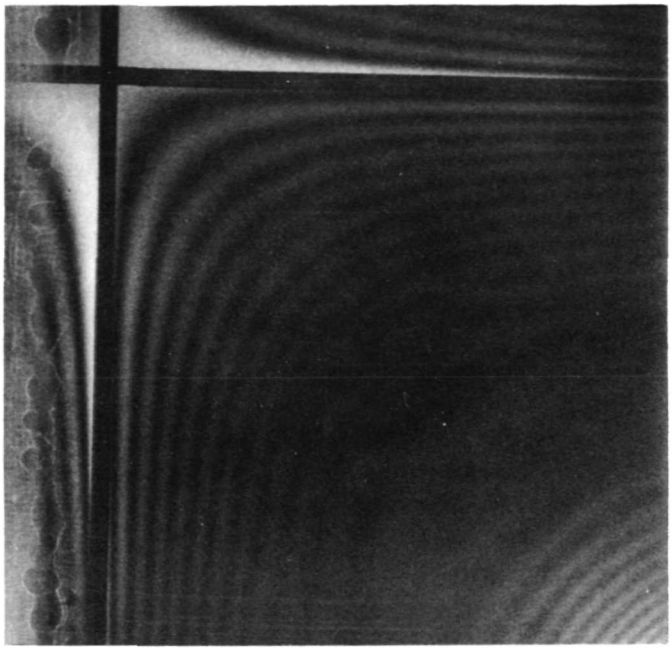

MODE SHAPE OF FIFTH MODE
$K_S = 400$, $\omega_5 = 740$ cps

FIGURE 20

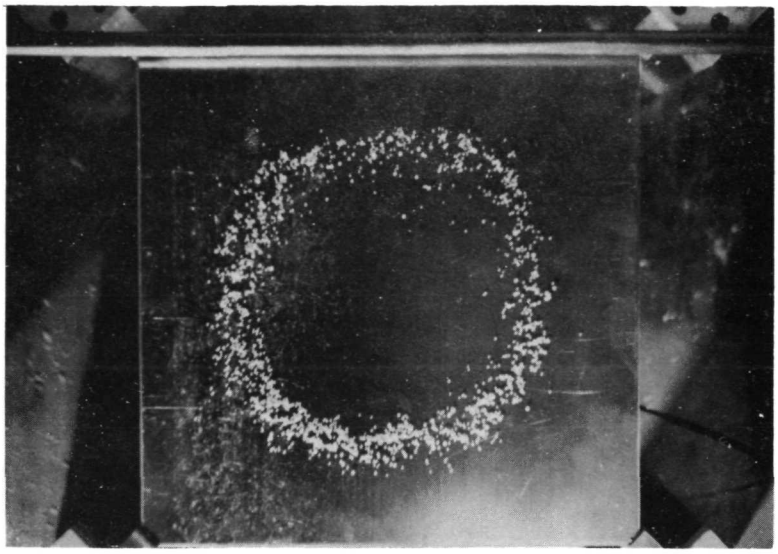

$K_s \approx 400 \quad \omega = 821$ cps

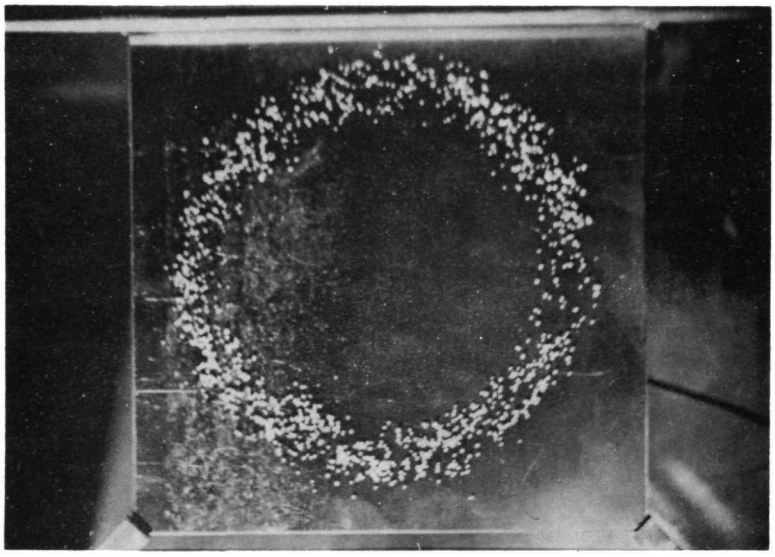

$K_s \approx 5 \quad \omega = 419$ cps

EFFECT OF SUPPORT STIFFNESS ON
MODE SHAPE, SIXTH MODE

FIGURE 21

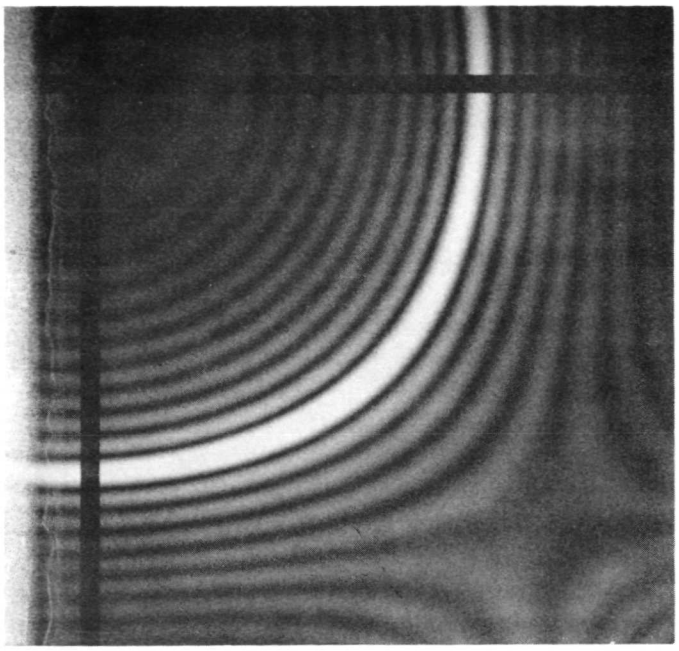

MODE SHAPE OF SIXTH MODE
$K_S = 400$ $\omega_6 = 850$ cps

FIGURE 22

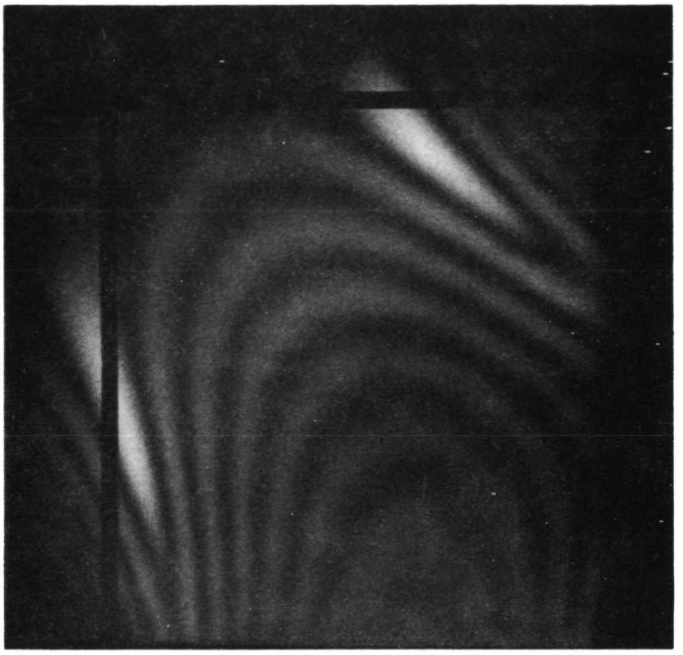

MODE SHAPE OF SEVENTH MODE
$K_S = 400$ $\omega_7 = 984$ cps

FIGURE 23

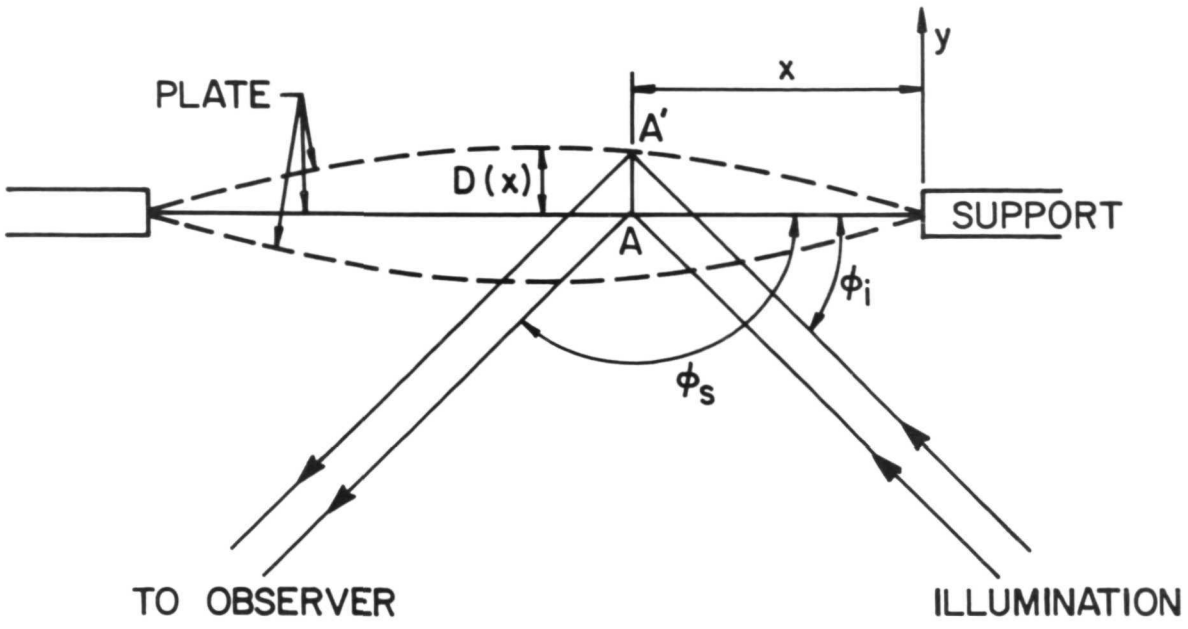

a) GEOMETRY OF HOLOGRAPHIC OPTICS FOR A VIBRATING PLATE

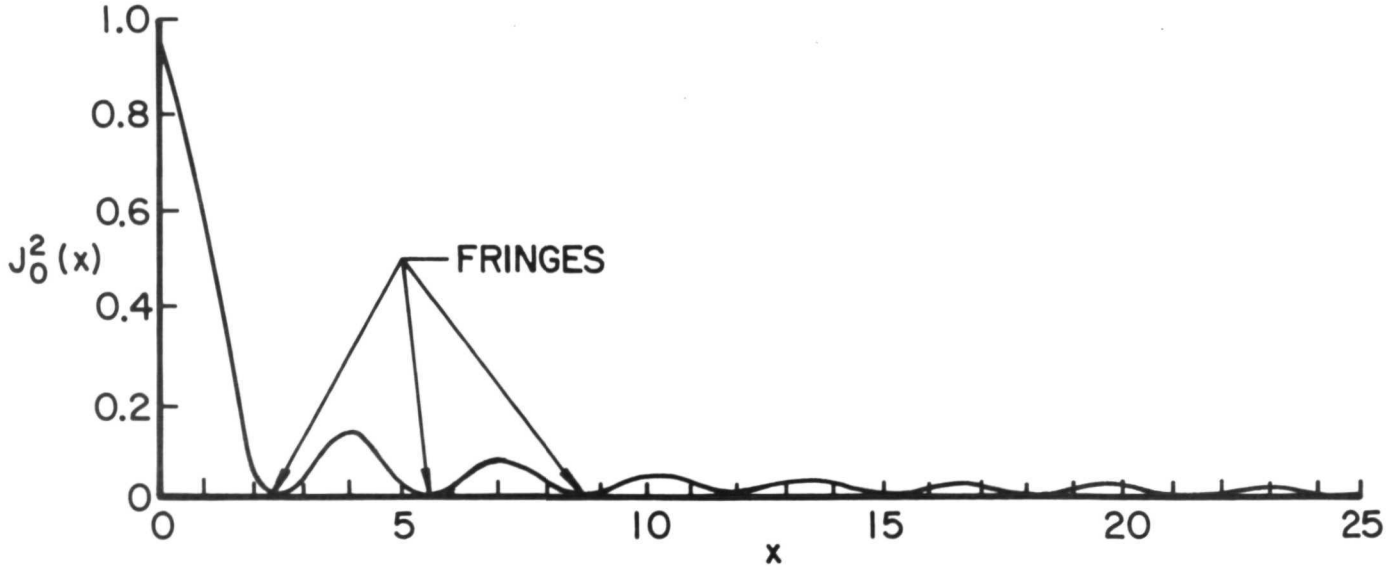

b) NON-DIMENSIONAL FRINGE INTENSITY
vs NON-DIMENSIONAL AMPLITUDE IN TERMS OF BESSEL FUNCTION

FIGURE 24

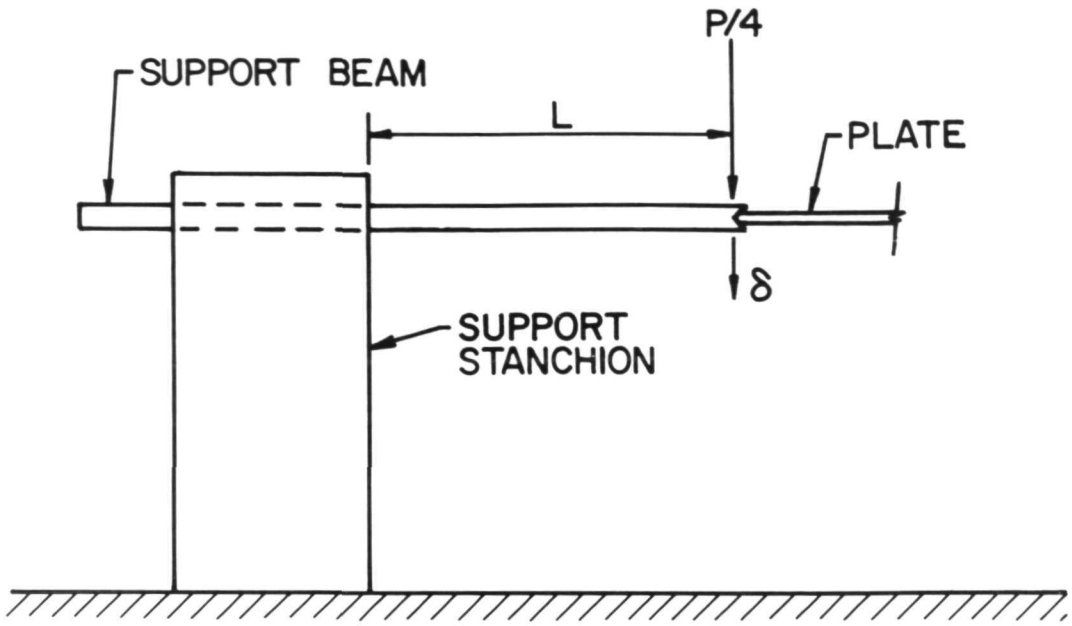

a) CALIBRATION LOAD CONDITION

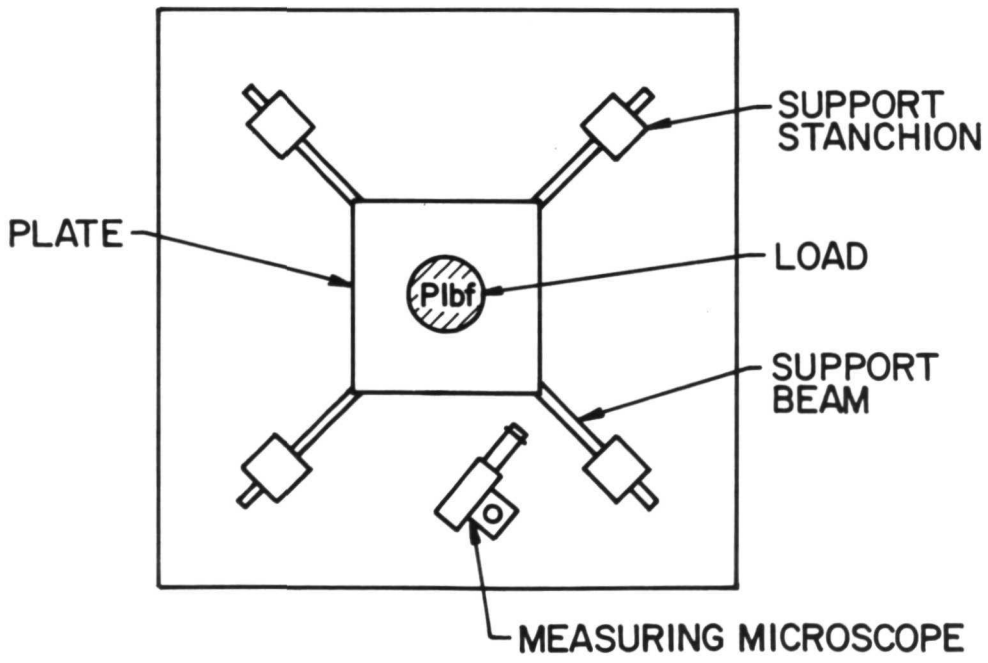

b) CALIBRATION SETUP

FIGURE 25

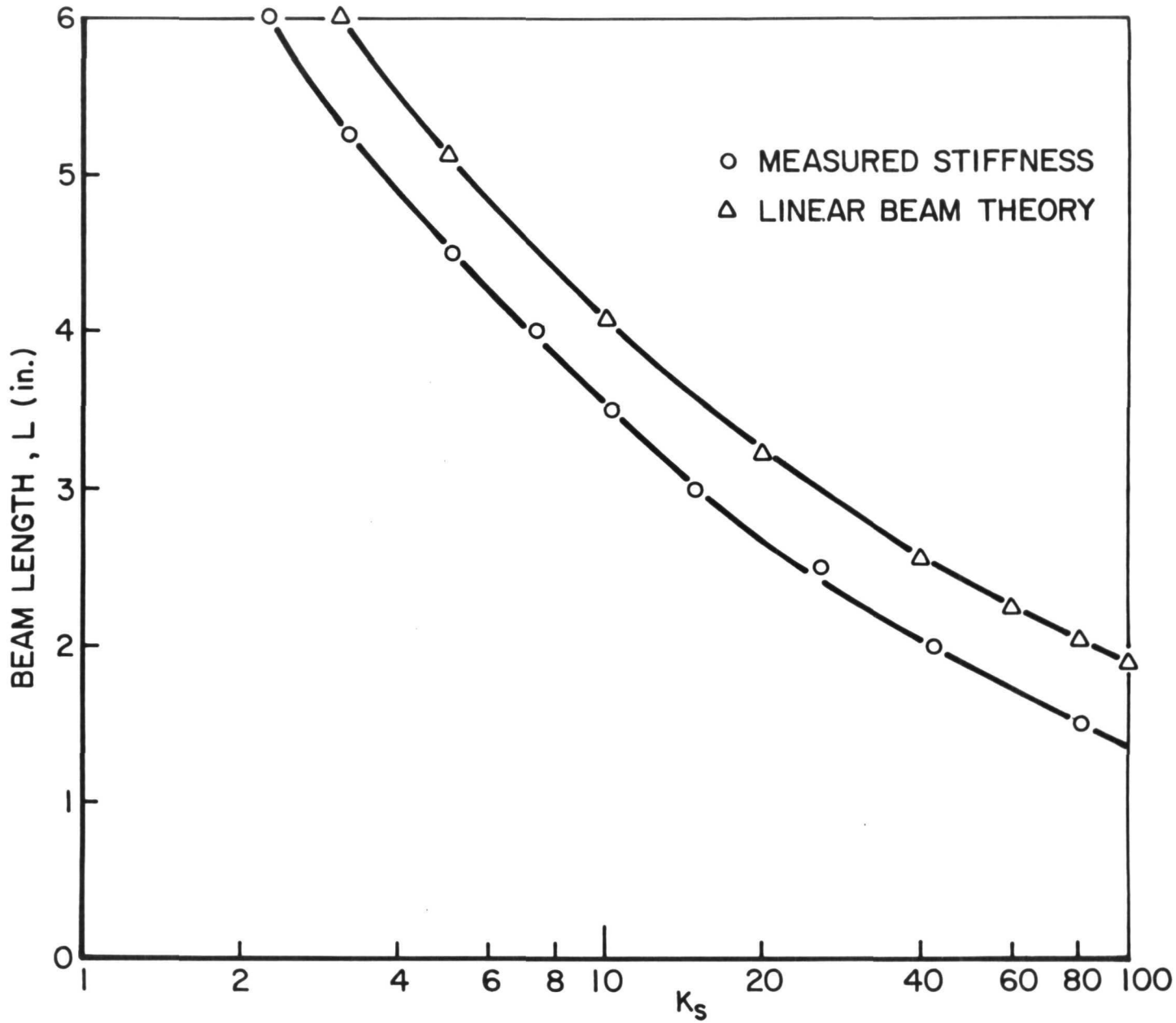

SUPPORT BEAM LENGTH vs SUPPORT STIFFNESS

FIGURE 26

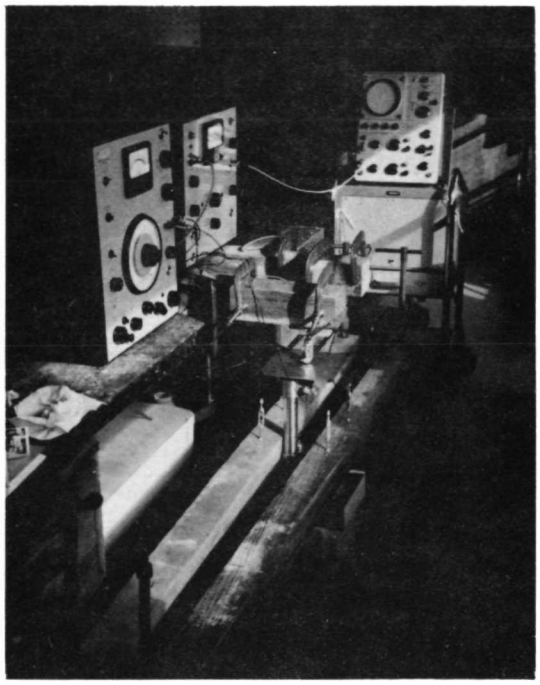

SUPPORT FRAMEWORK AND EQUIPMENT
FOR PRELIMINARY EXPERIMENT

FIGURE 27

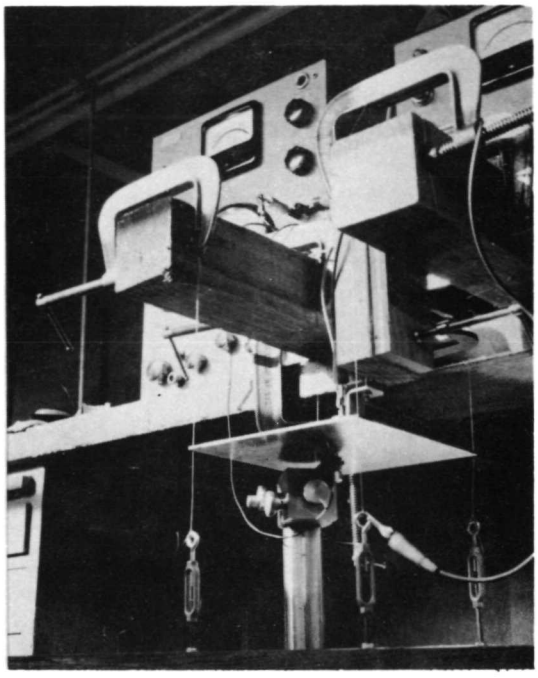

PLATE SUPPORTS FOR
PRELIMINARY EXPERIMENT

FIGURE 28

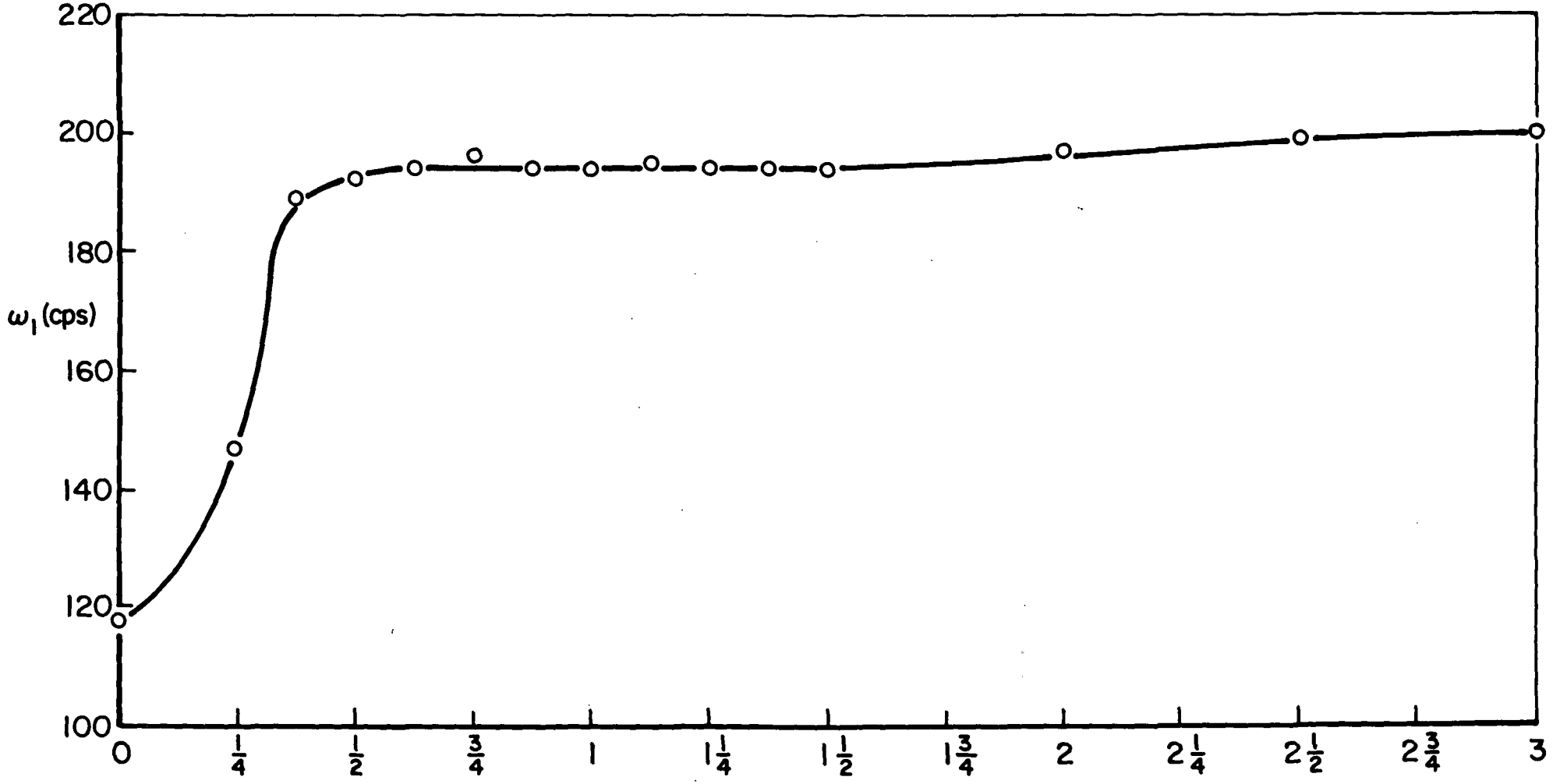

FREQUENCY vs SUPPORT TENSION, FIRST MODE

FIGURE 29

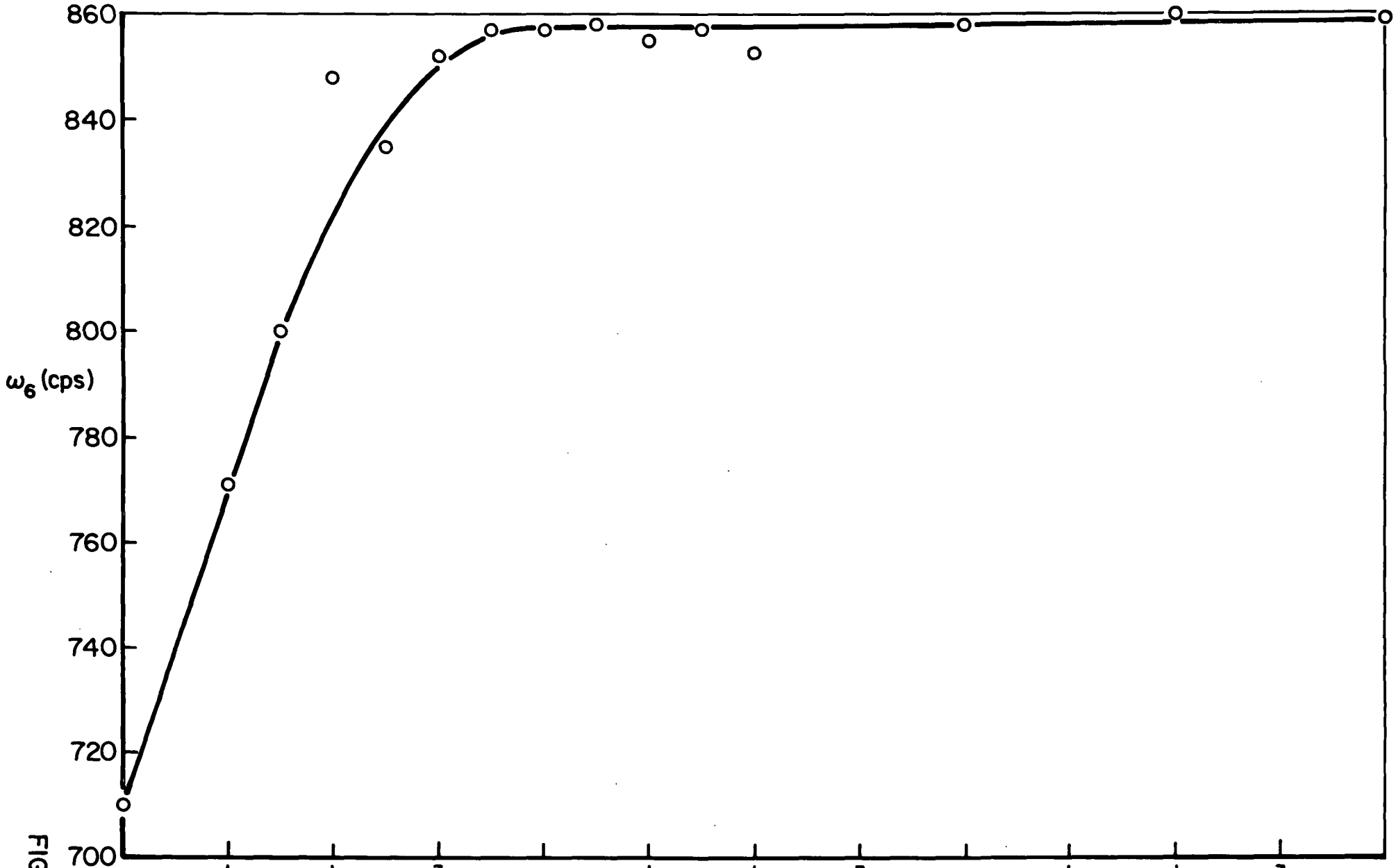

FIGURE 30

FREQUENCY vs SUPPORT TENSION, SIXTH MODE

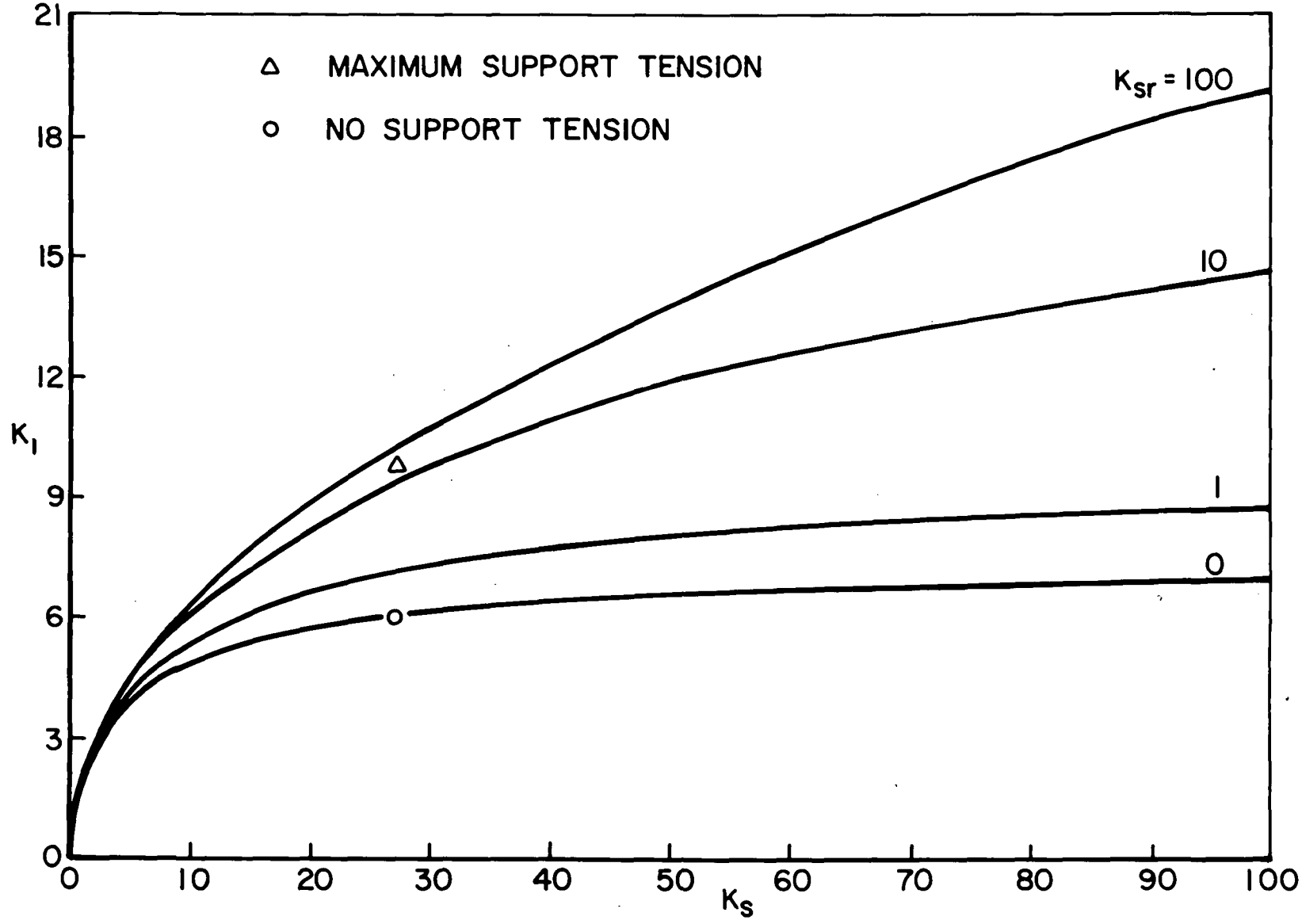

PRELIMINARY EXPERIMENT, FREQUENCY vs SUPPORT STIFFNESS, FIRST MODE

FIGURE 31

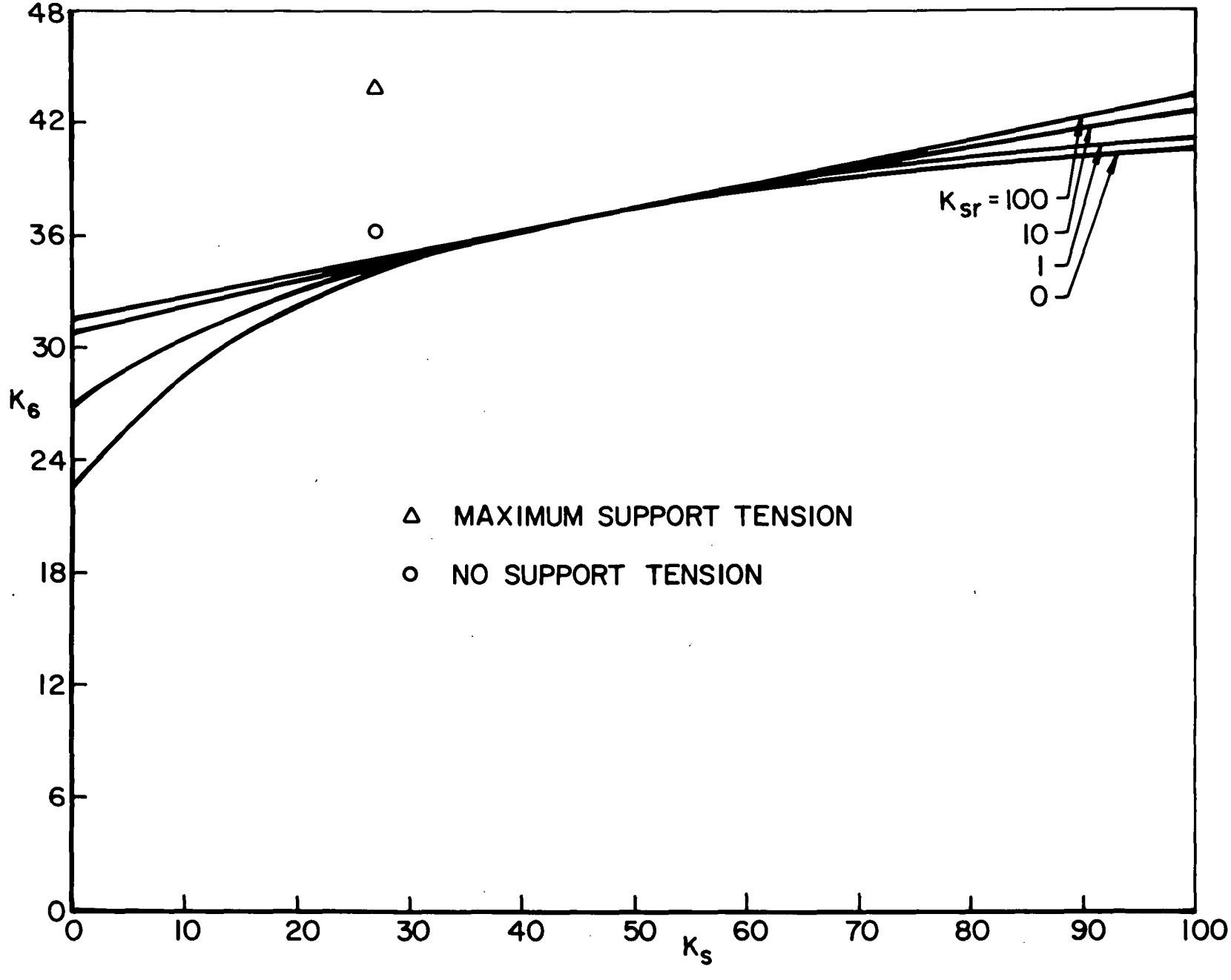

PRELIMINARY EXPERIMENT, FREQUENCY vs SUPPORT STIFFNESS, SIXTH MODE

FIGURE 32

APPENDIX A

EQUIPMENT LISTING

Frequency Analysis

1. Oscillator - Bruel and Kjaer, Type 1022
2. Magnetic transducer - Bruel and Kjaer, No. MM 0002
3. Capacitive pickup - Bruel and Kjaer, No. MM 0004
4. Microphone Amplifier - Bruel and Kjaer, Type 2603
5. Oscilloscope - Tektronix, Type 502
6. Measuring Microscope - Gaertner Scientific, No. M103

Mode Shape Analysis

1. Laser - Spectra - Physics Model 120, Helium-Neon C.W. Laser, 8 mw
2. Beam Splitter - Jodon Engineering Associates, Inc. UBA 200 Variable Beam Splitter
3. Prisms - A. Jaegers Optics
4. Spatial Filters - Jordon Engineering Associates, Inc. Model LPSF-100
5. Spectroscopic Plates - Kodak Type 649-F backed glass plates
6. Holographic Bench - One ton welded steel, pneumatic isolating

APPENDIX B

RAYLEIGH-RITZ ANALYSIS

The theoretical evaluation of the modal frequencies of the plate was performed by applying the Rayleigh-Ritz method to an energy approach utilizing Lagrange's Equations. The major part of this analysis is taken from Dowell[4].

Considering a flat plate, the elastic potential energy in cartesian coordinates is

$$U = \frac{1}{2}\iint\left[D_x\left(\frac{\partial^2 w}{\partial x^2}\right)^2 + D_y\left(\frac{\partial^2 w}{\partial y^2}\right)^2 + 2D_1\frac{\partial^2 w}{\partial x^2}\frac{\partial^2 w}{\partial y^2} + 4D_{xy}\left(\frac{\partial^2 w}{\partial x\,\partial y}\right)^2\right]dx\,dy \qquad \text{(B-1)}$$

where, for an isotropic plate

$$D_x = D_y = D$$
$$D_1 = \nu D$$
$$D_{xy} = \frac{(1-\nu)}{2} D$$

The kinetic energy is

$$T = \frac{1}{2}\iint m\left(\frac{\partial w}{\partial t}\right)^2 dx\,dy \qquad \text{(B-2)}$$

Applying a Rayleigh-Ritz approximation to the energy relations, expand the plate deflection

$$w = \sum_m q_m(t)\,\psi_m(x,y) \qquad \text{(B-3)}$$

Substituting this relationship into the energy expressions

$$U = \frac{1}{2} \sum_m \sum_n K_{mn} q_m q_n \tag{B-4}$$

$$T = \frac{1}{2} \sum_m \sum_n M_{mn} \dot{q}_m \dot{q}_n \tag{B-5}$$

where

$$K_{mn} = \iint \left[D_x \frac{\partial^2 \psi_m}{\partial x^2} \frac{\partial^2 \psi_n}{\partial x^2} + 2D_1 \frac{\partial^2 \psi_m}{\partial x^2} \frac{\partial^2 \psi_n}{\partial y^2} + D_y \frac{\partial^2 \psi_m}{\partial y^2} \frac{\partial^2 \psi_n}{\partial y^2} + 4D_{xy} \frac{\partial^2 \psi_m}{\partial x \partial y} \frac{\partial^2 \psi_n}{\partial x \partial y} \right] dx\,dy \tag{B-6}$$

$$M_{mn} = \iint m \psi_m \psi_n \, dx\,dy \tag{B-7}$$

In choosing the plate mode shapes, products of free-free beam modes were used due to the orthogonality of these modes, and the simplifications they introduced into the analysis. Let

$$\psi_m(x,y) = X_{m_x}(x) Y_{m_y}(y) \tag{B-8}$$

where $X_{m_x}(x)$ and $Y_{m_y}(y)$ are free-free beam modes in the x and y directions, and*

$$m_x = 1, \ldots \quad , \text{MMAX}$$

$$m_y = 1, \ldots \quad , \text{MRMAX}$$

$$m = 1, \ldots \quad , \text{MMAX x MRMAX}$$

*Due to the two-dimensional nature of the problem, for each mode number m, there exist two related indices m_x and m_y associated with each respective dimension.

Substituting (B-8) into (B-6) and (B-7)

$$K_{mn} = \iint \Big[D_x \frac{d^2 X_{m_x}(x)}{dx^2} \frac{d^2 X_{n_x}(x)}{dx^2} Y_{m_y}(y) Y_{n_y}(y)$$

$$+ 2D_1 \frac{d^2 X_{m_x}(x)}{dx^2} \frac{d^2 Y_{n_y}(y)}{dy^2} Y_{m_y}(y) X_{n_x}(x)$$

$$+ D_y \frac{d^2 Y_{m_y}(y)}{dy^2} \frac{d^2 Y_{n_y}(y)}{dy^2} X_{m_x}(x) X_{n_x}(x)$$

$$+ 4D_{xy} \frac{dX_{m_x}(x)}{dx} \frac{dY_{m_y}(y)}{dy} \frac{dX_{n_x}(x)}{dx} \frac{dY_{n_y}(y)}{dy} \Big] dx\,dy \qquad \text{(B-9)}$$

$$M_{mn} = \iint m X_{m_x}(x) Y_{m_y}(y) X_{n_x}(x) Y_{n_y}(y)\, dx\,dy \qquad \text{(B-10)}$$

In this analysis, the orthogonal mode shapes were choosen so that

$$\int X_{m_x}(x) X_{n_x}(x)\, dx = 0 \qquad m_x \neq n_x$$

$$= 1 \qquad m_x = n_x \qquad \text{(B-11)}$$

$$\int \frac{d^2 Y_{m_y}(y)}{dy^2} \frac{d^2 Y_{n_y}(y)}{dy^2} dy = 0 \qquad m_y \neq n_y$$

$$= C_{m_y} \qquad m_y = n_y \qquad \text{(B-12)}$$

Therefore, (B-9) and (B-10) can be simplified

$$M_{mn} = M \delta_{mn} \tag{B-13}$$

where M is the plate mass and δ_{mn} is the dirac delta function.

$$K_{mn} = D_x C_{m_x} \delta_{mn} + D_y C_{m_y} \delta_{mn} + \iint \left[2D_1 \frac{d^2 X_{m_x}(x)}{dx^2} \frac{d^2 Y_{n_y}(y)}{dy^2} Y_{m_y}(y) X_{n_x}(x) + 4 D_{xy} \frac{dX_{m_x}(x)}{dx} \frac{dY_{m_y}(y)}{dy} \frac{dX_{n_x}(x)}{dx} \frac{dY_{n_y}(y)}{dy} \right] dx\, dy \tag{B-14}$$

These generalized mass and stiffness terms are for the plate alone, but can easily be expanded to handle the support conditions. This analysis is concerned with the effect of point stiffnesses and masses on the natural modes of a plate. The energy due to these point support characteristics can be incorporated into the analysis as additional generalized mass and stiffness terms.

Consider a translational spring with stiffness k_s, located at a point (x_s, y_s). The elastic energy contribution of the spring will be

$$\frac{1}{2} k_s w^2(x_s, y_s) \tag{B-15}$$

The additional generalized stiffness term will be of the form

$$K^s_{mn} = k_s \Psi_m(x_s, y_s) \Psi_n(x_s, y_s) = k_s X_{m_x}(x_s) Y_{m_y}(y_s) X_{n_x}(x_s) Y_{n_y}(y_s) \tag{B-16}$$

If a point mass, m_s , was located at point (x_s , y_s) on the plate's surface, it would have a kinetic energy equal to

$$\frac{1}{2} m_s \left(\frac{\partial w(x_s, y_s)}{\partial t} \right)^2 \qquad \text{(B-17)}$$

The additional generalized mass term will be of the form

$$M^s_{mn} = m_s \Psi_m(x_s, y_s) \Psi_n(x_s, y_s)$$

$$= m_s X_{m_x}(x_s) Y_{m_y}(y_s) X_{n_x}(x_s) Y_{n_y}(y_s) \qquad \text{(B-18)}$$

It should be noted that neither the total generalized mass or stiffness matrices are necessarily symmetric. It is convenient to symmetrize these matrices in the following manner. Let

$$\tilde{K}_{mn} = \frac{K_{mn} + K_{nm}}{2}$$

$$\tilde{M}_{mn} = \frac{M_{mn} + M_{nm}}{2} \qquad \text{(B-19)}$$

These new mass and stiffness matrices are symmetric, and can be used in place of the unsymmetric matrices without changing the energy expressions as shown below

$$U = \frac{1}{2} \sum\sum K_{mn} q_m q_n$$

$$= \frac{1}{2} \left[\frac{1}{2} \sum\sum K_{mn} q_m q_n + \frac{1}{2} \sum\sum K_{nm} q_m q_n \right]$$

$$= \frac{1}{2} \sum\sum \tilde{K}_{mn} q_m q_n \qquad \text{(B-20)}$$

Thus, combining (B-16) and (B-18) with (B-13) and (B-14) and symmetrizing with (B-19), the energy expressions for the plate and its support system are

$$U = \frac{1}{2} \sum\sum \tilde{K}_{mn} q_m q_n$$

$$T = \frac{1}{2} \sum\sum \tilde{M}_{mn} \dot{q}_m \dot{q}_n \qquad \text{(B-21)}$$

Thus system equations can be obtained using Lagrange's equations

$$\frac{d}{dt}\left(\frac{\partial T}{\partial \dot{q}_u}\right) + \frac{\partial U}{\partial q_u} = 0 \qquad u = 1, \ldots MMAX \cdot MRMAX \qquad \text{(B-22)}$$

and (B-21) . They are

$$\sum_m \tilde{M}_{mu} \ddot{q}_m + \sum_m \tilde{K}_{mu} q_m \qquad u = 1, \ldots MMAX \cdot MRMAX \qquad \text{(B-23)}$$

or, in matrix notation

$$[\tilde{M}]\{\ddot{q}\} + [\tilde{K}]\{q\} = 0 \qquad \text{(B-24)}$$

To find the normal vibrational modes of the system, assume simple harmonic motion

$$\{q\} = \{\bar{q}\} e^{i\omega t}$$

therefore

$$\left(-\omega^2[\check{M}] + [\check{K}]\right)\{\check{q}\} = 0 \qquad \text{(B-25)}$$

Equation (B-25) can be treated as a standard eigenvalue problem and solved for the characteristic eigenvalues, plate frequencies, and eigenvectors, and plate mode shapes.

APPENDIX C

COMPUTER EVALUATION

The computer analysis used to predict the variation in the plate natural modes with support stiffness possessed some inherent difficulties which complicated the theoretical analysis. The primary difficulty was that for certain values of support stiffness, and depending on the number of beam modes used in the approximation, the program failed while attempting to handle small differences between large numbers.

All calculations were performed using double precision, so a more careful numerical evaluation of the problem would have involved a major overhaul of sophisticated mathematical techniques to solve the eigenvalue problem set up in Appendix B. Since the purpose of this investigation is primarily experimental, and the computer analysis was intended to be a reference point for the experimental results, the program was not rewritten. Instead, a calculation procedure was established which generated frequency vs. stiffness curves which were acceptable to the author, but which cannot be regarded as authoritative results. The agreement between the experimentally determined plate frequencies and the computer calculated predicted frequencies is very good, with the exception of the second symmetric-antisymmetric pair of modes, $K_{7,8}$. Considering the theoretical calculation procedure, it is likely that the computer analysis cannot predict higher modes accurately, and the observed discrepancy should not be attributed to a fault in the experimental apparatus.

The initial analysis did not subdivide the problem into doubly-symmetric, symmetric-antisymmetric, and doubly-antisymmetric plate modes. Consequently,

if m free-free beam modes were used in both the x and y directions, the first m^2 plate modes were analyzed. It was found that as m increased, the frequency of the fundamental mode did not converge to a limit as would be expected, but began to diverge as m exceeded eight beam modes.

It was assumed at this point that the lack of convergence was due to finite terms in the stiffness matrix which should be negligible for decoupled plate modes. The plate system was therefore physically uncoupled as previously described. Thus m symmetric beam modes in each direction were used to calculate m^2 doubly-symmetric plate modes. The fundamental frequency of the plate was again found to diverge when four symmetric modes were used in the calculation.

The fundamental mode diverged more rapidly with the number of modes for lower stiffnesses, than for rigid supports. Consider the eigenvalue problem for very low stiffness, $K_s = 1$. The matrix to be analyzed, $(-\omega^2[M] + [K])$, is shown below for $M = 2$

$$\begin{bmatrix} 4-\lambda & 7.5 & 7.5 & 117 \\ 7.5 & 515-\lambda & 14 & -42 \\ 7.5 & 14 & 515-\lambda & -42 \\ 117 & -42 & -42 & 4600-\lambda \end{bmatrix}$$

The first diagonal element is very small compared to the other diagonal elements. Since the system eigenvalues are related in magnitude to their corresponding diagonal elements, significant figures of the first eigenvalue are lost in the analysis due to the large size of the other diagonal elements

and corresponding eigenvalues. As m , and the size of the matrix, increases, the larger diagonal elements become increasingly more dominant, and the solution for λ_1 fails. For larger stiffnesses, the K_{11} element is larger compared to the other diagonal elements, and more modes must be added to drive the solution to divergence.

Once the nature of the problem was determined, a solution still needed to be found. Numerical techniques could be applied to the problem to equalize the size of the diagonal elements of the matrix under consideration. The standard eigenvalue routine should then be usable in solving for the plate frequencies. However, developing a general technique that would work for different matrix sizes and relative numerical values would prove to be a substantial amount of work for an experienced programmer.

Instead, the following analysis was applied. Leissa[8] gives the modal amplitude coefficients for the free plate modes. They are tabled below where A_{01} represents the relative amplitude of the combination of symmetric mode X_0 with antisymmetric mode Y_1.

K_5		K_4		K_6		$K_{7,8}$	
A_{11}	1.0	A_{00}	0.0	A_{00}	0.0	A_{01}	0.0
A_{13}	.0378	A_{02}	1.0	A_{02}	1.0	A_{03}	-.0682
A_{31}	.0378	A_{20}	-1.0	A_{20}	1.0	A_{21}	1.0
A_{33}	-.00435	A_{22}	0.0	A_{22}	-.0236	A_{23}	.0760

If two beam modes are used in each direction to calculate the system mass and stiffness matrices, then the first row and column of the matrices represent the combination of the first beam modes used in each direction, and the

fourth row and column represents the combination of the second beam modes used in each direction.

Looking at the mode shape coefficients in the above table, it can be seen that for the second doubly-symmetric (K_4) and first doubly-antisymmetric (K_5) modes, the fourth mode combination has negligible effect on the plate frequency, and the fourth row and column of the eigenvalue matrix can be eliminated in the computation. Thus for these modes, and also for the first doubly-symmetric and symmetric - antisymmetric modes, the fourth row and column of the mass and stiffness matrices have been eliminated from the four-by-four matrices for the eigenvalue calculation. However, for the third doubly-symmetric (K_6) and second symmetric-antisymmetric ($K_{7,8}$) modes, the fourth modal combination is significant, and entire four-by-four mass and stiffness matrices must be used in the eigenvalue computation. A comparison of the computer results with the free plate and rigid point support results presented in Leissa is presented in section 2.2.3.

The comparison with Leissa was close enough so that the computer program was not rewritten. There remains, however, a certain element of doubt regarding the computer output since convergence was never achieved.

As was previously mentioned in section 2.1.3, plate eigenvalues could not be calculated for the case of rigid point supports because the computer failed to converge to a value as the support stiffness increased. As K_s exceeds ten thousand, the fundamental frequency diverges. This problem can likewise be traced to the computer losing significant figures in the eigenvalue analysis when it attempts to evaluate small differences between large numbers for very large stiffnesses. The rigid support plate frequencies could be guessed at from the frequency trend with increasing stiffness,

but since this experiment is concerned with the transition to zero support stiffness, the high stiffness region is not of interest and was ignored. At some point, it would be desirable to change the computer program so large numbers of modes and large stiffnesses can be employed, but this was not deemed necessary to the completion of this research.

APPENDIX D

SUPPORT STIFFNESS CALIBRATION

This section presents the calibration of the bending stiffness of the support beams as a function of the length of the beam. It would be both difficult and inconvenient to determine the magnitude of the support stiffness whenever the position of support stanchions is changed. The support stiffness is therefore measured for different support beam lengths, which is the parameter measured when the elasticity of the plate supports is altered.

In this experiment, the vertical spring supporting the plate is actually the bending stiffness of the horizontal support beams. Linear beam bending theory can be used to obtain an approximate stiffness vs. length curve, and this theoretical curve was used to design the support beams to obtain the desired stiffness range for the experiment. The theoretical result

$$k = \frac{3EI}{L^3}$$

is plotted on Figure 26 along with the measured calibration curve.

The actual procedure used to measure the support stiffness for a given support beam length is as follows. The four support stanchions were locked to the base plate at a distance L from the corners of the experimental plate. The support beams were then clamped to the stanchions so that the projecting length of the beam was (L + 1/8) inches. The reason for the additional eighth-inch is that when the plate is inserted into the routed angles in the support beams, the top edge of each beam overlaps the plate by 1/8" (see Fig. 5). The plate was therefore effectively supported by beams of length L .

The plate was then fastened into the supporting structure, and a measuring microscope focused on a point on one of the support beams directly under the corner of the plate. A load P was then placed on the center of the plate, and the vertical deflection of the support beam, δ, measured with the travelling microscope. The calibration setup is illustrated in Fig. 25b.

Since the total load must be carried by the four supports, the stiffness of each beam is:

$$k = \frac{P/4}{\delta}$$

The beam deflection was measured for different beam lengths, L, and for different values of the plate load for each L. The average measured stiffness for each beam length was then calculated, and the results are presented in Fig. 26. This measured stiffness curve is in qualitative agreement with theoretical curve, but there is a significant quantitative difference. It appears that for a given stiffness K_s, the experimental measurement of the beam length is approximately 1/2" less than the theoretically calculated length. This relationship holds over the entire range of stiffness considered.

As can be seen from the photograph of the apparatus, Fig. 2, the forward set screw which physically clamps the support beam to the support stanchion is located 1/4" inboard of the front edge of the stanchion cover plate. It therefore appears that the support beam is not effectively clamped by the cover plate, but by the set screw. This has the effect of adding another 1/4" of flexibility to the support beam. It is reasonable to assume that the remaining quarter-inch difference between linear beam bending theory and

the experimentally measured support stiffness curve is similarly traceable to the manner in which the support beam is clamped to the stanchion.

During the course of the experimental investigation, the support beams were fastened to the stanchions in the same manner employed in this calibration, and the equivalent non-dimensional stiffness parameter was determined from the experimental curve in Fig. 26.

APPENDIX E

PRELIMINARY EXPERIMENT

The initial design of the experiment utilized the compressive stiffness of long, thin rods as the elastic plate supports. Four wires would be attached to the corner of the plate, and the plate would hang suspended from these wires, which would be clamped into a supporting framework. The support stiffness would be varied by changing the length of the wire which supported the plate.

There were several obvious advantages which inspired this design. To fasten the support wires to the plate, 0.02" diameter holes were drilled in the corners of the plate 1/8" from both sides. Set screws were placed in the plane of the plate to fasten the wires into these holes. This is a fairly reasonable approximation to corner-point supports, and is sufficiently permanent, unlike the support beam method. Thin support wires would be flexible enough so rotation at the plate corners would be allowed. Although the supports would not be located exactly at the corners, their inboard position would raise the plate frequencies by no more than one or two percent.

The most desirable feature of this design is that the support stiffness is directly related to the wire length. The compressive stiffness of a beam is:

$$k = \frac{AE}{L}$$

If fairly uniform wire is used, the product AE will be a constant and can be experimentally measured. Therefore:

$$C = (AE)_{effective}$$

$$k = \frac{C}{L}$$

To half the support stiffness, simply double the length of the wires supporting the plate. Varying the support stiffness is therefore very easy. The clamp holding each support wire to the support framework may be loosened, the wire let out to the proper length, and then clamped. The next support wire may be adjusted independently of the other wires. With horizontal support beams, all the beams must be adjusted in unison to support the plate.

There are several disadvantages to this model, some foreseen, and others discovered during experimentation. In order to test the feasibility of this configuration, a rough model was constructed and tested. (See Figs. 27 and 28) Four-by-fours were clamped across a workbench top and to the bottom drawers of the bench to provide an approximately rigid framework. Four steel wires diameter = 0.022", were fastened to the wooden beams with "c" clamps, and a 8" by 8" by 1/8" aluminum plate was hung from the wires. The plate was driven from below by a magnetic transducer, and the plate response was observed on an oscilloscope as the output of a capacitive pickup suspended over the plate.

Two major problems were encountered immediately. Firstly, the weight of the plate did not apply enough tension to the support wires to make them hang straight with no kinks. Prestressing the wires would not remove the bends in the wires so the plate would hang flat. It was further observed that the transverse bending frequency of the wire was within the frequency range of the plate response. Both these problems would be solved by applying an initial tension to the support wires. Tension would straighten the support wires, and would not change the compressive stiffness of the wires if the tension was not large enough for the wires to behave in a nonlinear manner. Tension will also raise the bending frequency of the wires through

the relation

$$\omega = \frac{1}{2L}\sqrt{T/\mu}$$

The experiment was therefore modified so that the support wires ran through the plate and were fastened to turnbuckles on the lower four-by-fours (see Fig. 28). Tests showed however, that the fundamental frequency of the plate was altered by the support tension. Before this configuration was abandoned in favor of horizontal beam supports, the variation of frequency with support tension was investigated.

The wire constant was measured, and its value was determined to be

$$C = (AE)_{effective} = 9910 \quad lbf$$

The average length of the four support wires was measured at

$$L = 10\tfrac{7}{8}"$$

This corresponds to a non-dimensional stiffness of

$$K_s = 26.9$$

The plate was excited at its center, so that the two primary modes excited would be the first and third doubly symmetric modes, which are classified as the first and sixth plate modes in this experiment.

The turnbuckles were left completely loose so there was no tension on the support wires. The frequencies of the two modes were measured, then all four turnbuckles were rotated a quarter turn. The frequencies were again measured, and the procedure repeated until the modal frequencies had reached asymptotic values. The results are presented in Figs. 29 and 30.

Because of the non-rigidity of the support framework, it was not possible to calibrate the actual tension applied by a full rotation of the turnbuckle, but there appeared to be a large amount of tension in the support wires by

the time that the modal frequencies achieved constant values. With a large amount of tension in the support wires, the wires going through the plate corners were taut, and the plate was constrained to a condition of no rotation at the corners. Applying tension to the support wires had the same effect as adding rigid rotational springs at the corners.

This assumption was checked by computer analysis. Figures 31 and 32 show the variation of the first and sixth plate mode frequencies versus support stiffness for different values of corner rotational stiffness. The curve $K_{sr} = 100$ approximates the condition of rigid rotational springs. The measured plate frequencies for zero, and for maximum tension are plotted on these curves for the measured support stiffness, $K_s = 26.9$.

For the fundamental mode, both the zero tension and maximum tension cases (zero and rigid rotational springs) agree with the theoretical curves to within the accuracy limits of this experiment. The sixth mode does not behave correctly, however. For the given value of the support stiffness, adding rotational stiffness should have little effect on the frequency. When tension was applied to the supports, however, the frequency of the sixth mode jumped 20% from the no tension value, which was only 7% higher than the theoretical calculation.

This unpredicted frequency shift implied that the wire support model was still not completely under control, and the design was abandoned in favor of the horizontal support beam configuration. Considering the inpromptu manner in which this preliminary experiment was constructed, the zero-tension frequencies compare relatively well with the theoretical results. A more carefully constructed apparatus of this sort could be used for an experimental investigation involving discrete elastic supports. The only major problem

would be dealing with the transverse vibration frequencies of the support wires, which might not have a large effect on the plate modes due to the very small mass of the support wires. This assumption may be unjustified and should probably be checked out experimentally.

APPENDIX F

HOLOGRAPHIC THEORY

An introduction to the basic theory behind holography is necessary in developing time-averaging theory. Holography involves the recording on a photographic plate of the interaction between an optical reference beam, and an object beam which is diffused by the surface of the object under observation. The photographic plate, which becomes the hologram, records the intensity of the combined light from the two beams which impinges on its surface. The intensity of the total light beam varies across the plane of the hologram, and is a maximum when the object and reference beams are in phase and add their intensities. Similarly, the intensity is a minimum when the two beams are out of phase and their amplitudes cancel. When the photographic plate is developed, it becomes a complex diffraction grating which stores the phase and amplitude relationships of the object beam. Thus when only the reference beam is directed through the hologram, it is diffracted, and the original wavefront from the object is completely reconstructed. This reconstructed wavefront is indistinguishable from the original object beam, and produces a three-dimensional virtual image of the object at the object's original position.

Holographic interferometry has proven to be a useful process in detecting small deformations. Since the hologram stores phase information from the object beam, it is capable of detecting small changes in the object's position on the order of one wavelength of the illuminating light.

For double-exposure holography, consider the deflection of a cantilevered beam under an end load. If the exposure time of the holographic

plate is $2t$ minutes, expose the plate to light reflecting off the deformed beam for t minutes, then load the end of the beam and expose the plate for another t minutes. The hologram superimposes the phase information from these two wavefronts, and the reference beam will reconstruct the composite wave after the hologram is developed. At the base of the beam, where there is no deflection, the two wavefronts are identical. Further up the beam, it will have deflected a distance Δ from its original position. When

$$\Delta = (2m-1)\lambda/4 \qquad m = 1, 2, \ldots n \qquad \text{(F-1)}$$

where λ is the wavelength of the light source, the deformed and undeformed wavefronts from these points are out of phase, and a dark interference fringe will appear across the beam where this condition on Δ holds. If the wavelength of the laser light is known, the deflection of the beam can be measured by counting the number of fringes, m, and using equation (F-1).

Time-average holography is an extension of double-exposure holography. Consider a plate vibrating in a normal mode. Each point on the plate moves sinusoidally with an amplitude $d(x,y)$. It is intuitively obvious that the point spends more time near this position of maximum deflection, where the velocity is zero and the point comes to rest, then it does at an intermediate point between its two extremes, where the plate is moving with a finite velocity. If a hologram is made of this vibrating object over a period of time equivalent to several cycles of the plate, then the photographic plate will record the "time-average" position of each point on the vibrating surface. Since

each point is at its maximum deflection positions for a longer period of time than it is at any of its intermediate positions, the hologram will tend to record the position of each point predominantly at its positive and negative maximum amplitude positions. Thus the hologram of the vibrating surface will approximate a double exposure hologram of the plate taken at its two maximum amplitude positions.

Although the actual hologram will be more complicated than this, it will behave qualitatively like the double-exposure hologram just described. It will exhibit fringe patterns, where each fringe represents the displacement at that point between the two extreme positions of the point. Thus interference fringes are formed, each fringe being a contour line of equal displacement of the vibrating surface. The nodal lines of the vibrational mode will be observable as zero order fringe contours, and the maximum displacement of the surface will be marked by the largest observable fringe order. As will be shown mathematically, the zero order fringe contour is the bright contour of maximum intensity.

A mathematical relationship can be derived relating the vibration amplitude of a point on a vibrating surface to the intensity of the fringe pattern at that point. The analysis presented here is a shortened version of that presented by Collier, Burchkhardt and Lin[9] in section 15.4.1 of their book. For a more detailed analysis of time-average holography, this reference is recommended.

Consider a surface undergoing simple harmonic motion. The displacement of an arbitrary point can be written as

$$D(x,t) = D(x)\cos\omega t \qquad \text{(F-2)}$$

if ω is the frequency of vibration of the surface, and the surface is simplified to exclude vibration in the Y direction. A geometric analysis of the optical path of the reflected object beam shows that the instantaneous phase shift of the scattered light rays is

$$\delta(x,t) = -\left(\frac{2\pi}{\lambda}\right) D(x)\cos\omega t\left[\sin\phi_i + \sin\phi_s\right] \qquad \text{(F-3)}$$

where λ is the wavelength of the laser light and ϕ_i and ϕ_s are the angles made with the surface by the incoming and scattered beams.

Let $\tilde{r}$ and $\tilde{s}(x,t)$ represent the complex amplitudes of the reference and object beams, and let $\tilde{r}^*$ and $\tilde{s}^*(x,t)$ be their complex conjugates. The intensity of the combined light beam reaching the photographic plate is

$$I(x,t) = \tilde{s}(x,t)\tilde{s}^*(x,t) + \tilde{r}\tilde{r}^* + \tilde{s}^*(x,t)\tilde{r} + \tilde{s}(x,t)\tilde{r}^* \qquad \text{(F-4)}$$

The photographic plate is exposed to the time-average of the intensity.

$$\langle I\rangle = \frac{1}{T}\int_0^T I(x,t)\,dt \qquad \text{(F-5)}$$

Integrating over one vibrational period, $T = 2\pi/\omega$

$$\langle I\rangle = \frac{1}{T}\int_0^T\left[\tilde{s}(x,t)\tilde{s}^*(x,t) + \tilde{r}\tilde{r}^* + \tilde{s}^*(x,t)\tilde{r}\right]dt + \frac{\tilde{r}^*}{T}\int_0^T \tilde{s}(x,t)\,dt \qquad \text{(F-6)}$$

The second integral, which contains the original object beam, modified by the conjugate of the reference beam, is the source of the holographic virtual image, and the first integral will henceforth be disregarded.

If the transmittance of the developed hologram is proportional to the time-averaged intensity, then when the hologram is illuminated by the original reference beam, the observed virtual image of the object will be reconstructed by the wave

$$\tilde{w} \propto \tilde{r} \frac{\tilde{r}^*}{T} \int_0^T \hat{s}(x,t)\, dt$$

$$\propto \frac{1}{2\pi} \int_0^{2\pi} \tilde{s}(x,t)\, d(\omega t) \qquad \text{(F-7)}$$

This equation represents the light from any point on the vibrating surface, and the wavefront from the object at an arbitrary distance from the vibrating surface. Let $\tilde{a}(x,t)$ represent the complex amplitude of the light arriving at observation point P from point A on the vibrating surface. Define the complex amplitude to be

$$\tilde{a}(x,t) = \tilde{a}(x) \exp\left[i\, \delta(x,t)\right] \qquad \text{(F-8)}$$

where $\tilde{a}(x)$ is the complex amplitude at P when the surface is in its undeformed position, and $\delta(x,t)$ is the phase difference produced by the surface displacement $D(x,t)$.

Now substitute $\tilde{a}(x,t)$ for $\tilde{s}(x,t)$ in equation (F-7)

$$\tilde{w}_A \propto \tilde{a}(x) \frac{1}{2\pi} \int_0^{2\pi} \exp\left[i\, \delta(x,t)\right] d(\omega t) \qquad \text{(F-9)}$$

This integrai represents interference at point P from the undisplaced

point A with the displaced positions of A during the vibration cycle. Substitute equation (F-3) into equation (F-9) and evaluate the integral

$$\frac{1}{2\pi}\int_0^{2\pi} \exp\left[i\,\delta(x,t)\right] d(\omega t)$$

$$= \frac{1}{2\pi}\int_0^{2\pi} \exp\left[-i\,\frac{2\pi}{\lambda}\,D(x)(\sin\phi_i + \sin\phi_s)\cos\omega t\right] d(\omega t)$$

$$= J_0\left[\frac{2\pi}{\lambda}\,D(x)(\sin\phi_i + \sin\phi_s)\right] \qquad \text{(F-10)}$$

where J_0 is the zero-order Bessel function. The light intensity at will be

$$\tilde{w}_A\,\tilde{w}_A^* \propto \tilde{a}(x)\tilde{a}^*(x)\left\{J_0\left[\frac{2\pi}{\lambda}\,D(x)(\sin\phi_i + \sin\phi_s)\right]\right\}^2 \qquad \text{(F-11)}$$

Equation (F-11) demonstrates that dark fringes in the observed interference pattern of the vibrating membrane correspond to displacements $D(x)$ such that

$$J_0^2\left[\frac{2\pi}{\lambda}\,D(x)(\sin\phi_i + \sin\phi_s)\right] = 0 \qquad \text{(F-12)}$$

Similarly, bright fringes in the interference pattern correspond to local maxima of this function. The intensity of the bright fringes is proportional to the magnitude of these maxima, which decrease as the argument of the function increases (see Fig. 24b). Thus as the displacement increases, the intensity

of the fringe pattern decreases. Nodal lines of zero displacement can therefore be identified as fringes of maximum brightness. By evaluating the Bessel function, the peak-to-peak vibration amplitude of any point on the object can be determined by observing the local fringe order of a time-averaged hologram.